AGU PUBLICATIONS

JGR

Journal of Geophysical Research: Solid Earth

RESEARCH ARTICLE
10.1002/2013JB010718

Key Points:
- Accurate depths were determined for Mariana trench earthquakes
- Deeper extensional trench earthquakes occurred at Central Mariana
- Indications for compressional stress were identified at Southern Mariana

Supporting Information:
- Readme
- Texts S1–S4, Figures S1–S26, Table S1

Correspondence to:
E. L. Emry,
ele11@psu.edu

Citation:
Emry, E. L., D. A. Wiens, and D. Garcia-Castellanos (2014), Faulting within the Pacific plate at the Mariana Trench: Implications for plate interface coupling and subduction of hydrous minerals, *J. Geophys. Res. Solid Earth*, *119*, 3076–3095, doi:10.1002/2013JB010718.

Received 24 SEP 2013
Accepted 14 MAR 2014
Accepted article online 18 MAR 2014
Published online 8 APR 2014

Faulting within the Pacific plate at the Mariana Trench: Implications for plate interface coupling and subduction of hydrous minerals

Erica L. Emry[1,2], Douglas A. Wiens[2], and Daniel Garcia-Castellanos[3]

[1]Now at Department of Geosciences, Pennsylvania State University, University Park, Pennsylvania, USA, [2]Department of Earth and Planetary Sciences, Washington University, St. Louis, Missouri, USA, [3]Instituto de Ciencias de la Tierra Jaume Almera, CSIC, Barcelona, Spain

Abstract We investigate faulting within the incoming Pacific plate at the Mariana subduction trench to understand stresses within the bending plate, regional stresses acting upon the plate interface, and the extent of possible faulting-induced mantle serpentinization. We determine accurate depths by inverting teleseismic *P* and *SH* waveforms for earthquakes occurring during 1990–2011 with Global Centroid Moment Tensor (GCMT) solutions. For earthquakes with M_w 5.0+, we determine centroid depths and source time functions and refine the fault parameters. Results from Central Mariana indicate that all earthquakes are extensional and occur at centroid depths down to 11 km below the Moho. At the Southern Mariana Trench, extensional earthquakes continue to 5 km below the Moho. One compressional earthquake at 34 km below the seafloor suggests stronger plate interface coupling here. In addition, we model the stress distribution within the Pacific plate along two bathymetric profiles extending seaward from the Mariana subduction trench axis to better understand whether our earthquake depth solutions match modeled scenarios for plate bending under applied external forces. Results from our flexure models match the locations of extensional and compressional earthquakes and suggest that the Pacific plate at Southern Mariana is experiencing larger, compressional stresses, possibly due to greater interplate coupling. Additionally, we conclude that if extensional faulting promotes the infiltration of water into the subducting plate mantle, then the top 5–15 km of the Pacific plate mantle are partially serpentinized, and a higher percentage of serpentinization is located near the Central Mariana trench where extensional events extend deeper.

1. Introduction

The cycling of water into subduction zones is important to subduction arc and back-arc volcanics [*Gill*, 1981; *Plank and Langmuir*, 1993; *Rüpke et al*., 2004], plate interface slip behavior [e.g., *Moore and Vrolijk*, 1992; *Shelly et al*., 2006; *Audet et al*., 2009], intermediate depth earthquakes [*Raleigh and Paterson*, 1965; *Meade and Jeanloz*, 1991], water exchange between the Earth's surface and mantle [*Rüpke et al*., 2004], composition of the Earth's mantle [*Thompson*, 1992; *Hirschmann*, 2006], and initiation of plate tectonics [*O'Neill et al*., 2007]. The amount of water input at the trench is unconstrained for many subduction zones, due to unknown amounts of lower crustal and upper mantle hydration [*Jarrard*, 2003; *Hacker*, 2008]. The amount of hydrated (serpentinized) oceanic mantle is particularly important for water expulsion processes deep within subduction zones, at arc and at subarc depths [*Hacker*, 2008; *Van Keken et al*., 2011].

Faulting within bending oceanic plates at subduction zone trenches, hereafter referred to as the outer rise, is an important pathway by which water is transported into the Earth. These faults result from flexural stress when ocean lithosphere bends at subduction zone trenches [*Isacks et al*., 1968; *Chapple and Forsyth*, 1979]. The presence of an outer rise bulge is characteristic of elastic plate flexure [*Caldwell et al*., 1976]; however, the occurrence of earthquakes within the plate is an indication that it is not entirely elastic but is also experiencing permanent deformation within the top of the plate [*Chapple and Forsyth*, 1979; *Goetze and Evans*, 1979]. Because mantle hydration is expected to be limited to the top of the oceanic plate where extensional, brittle failure occurs [e.g., *Ranero et al*., 2003; *Lefeldt et al*., 2009], the distribution of stress within the bending oceanic plate may allow us to estimate water storage potential of the subducting lithosphere.

In addition to stress created by plate flexure [*Caldwell et al*., 1976; *Chapple and Forsyth*, 1979], interplate locking at strongly coupled subduction zones may impact the stress distribution within the bending plate

[*Christensen and Ruff*, 1988]. At strongly coupled margins, outer rise earthquakes are temporally linked to large plate interface earthquakes [*Christensen and Ruff*, 1988]. As first observed by *Stauder* [1968] in the Rat Islands, extensional outer rise earthquakes occur more frequently after large, megathrust earthquakes. This observation along with the occurrence of compressional outer rise earthquakes prior to megathrust rupture was suggested by *Christensen and Ruff* [1988] to be characteristic of strongly coupled subduction zones. However, at weakly coupled or uncoupled subduction zones, no compressional outer rise earthquakes occur, and extensional outer rise events are not related to the subduction plate interface [*Christensen and Ruff*, 1988]. These observations suggest that the stress distribution within the bending oceanic plate at strongly coupled margins changes with time in response to the megathrust seismic cycle, in which case, the depth extent of water infiltration and mantle hydration may also change with time.

Because the maximum depth of mantle hydration is thought to be coincident with the location of the neutral plane, where plate-bending stresses switch from deviatoric tension to deviatoric compression, recent studies have determined the depth of the neutral plane as a means to infer depth of mantle hydration [*Lefeldt et al*., 2009]. At the Nicaragua outer rise, the depth of the neutral plane inferred from earthquake focal mechanisms [*Lefeldt et al*., 2009] corresponds well with a region of low mantle *P* wave velocities, suggestive of mantle serpentinization [*Van Avendonk et al*., 2011].

The Mariana subduction zone has long been cited as a water-rich system due to the prevalence of fore-arc serpentinite mud volcanoes [*Fryer et al*., 1999], water-rich arc lavas [e.g., *Shaw et al*., 2008; *Kelley et al*., 2010], and a serpentinized mantle wedge [*Tibi et al*., 2008; *Pozgay et al*., 2009; *Barklage*, 2010; *Pyle et al*., 2010], yet the initial amount of water stored within the Pacific plate mantle is unknown. This results in large uncertainties in amount of subducted water and the water budget of the Mariana subduction zone. Here we explore faulting within the Pacific plate at the Mariana subduction zone by inverting *P* and *SH* waves from outer-rise earthquakes in order to obtain more accurate centroid depths for these shallow events. We then compare the distribution of earthquake depths and focal mechanisms with two-dimensional finite-difference models of the stress distribution within the bending Pacific plate seaward of the Mariana Trench to help understand how deeply extensional stresses extend into the Pacific plate. These results are interpreted in terms of the likely hydration depths of the Pacific plate as well as possible variations in seismic coupling along the Mariana Trench.

2. Background

2.1. Faulting and Hydration of Incoming Oceanic Plates

Bathymetric observations of horsts and grabens within incoming plates at subduction zone trenches give strong evidence for faulting induced by plate bending [e.g., *Ranero et al*., 2003; *Oakley et al*., 2008; *Gardner*, 2010], and multichannel seismic reflection (MCS) studies have shown that at some subduction zones, faults exposed at the surface continue to mantle depths [*Ranero et al*., 2003]. In regions where preexisting faults on the incoming plate (seafloor fabric) strike nearly parallel to the trench axis, plate bending is accommodated by fault reactivation, whereas new faults form more readily where seafloor fabric converges at a high angle with the trench axis [*Masson*, 1991; *Ranero et al*., 2005]. *Ranero et al*. [2003] found that where seafloor fabric is subparallel to the trench axis, faults persist deeper into the bending oceanic plate than where new seafloor faults form, indicating that depth of outer rise faulting may be dependent on preexisting structure of the oceanic plate.

Global and regional surveys of outer rise seismicity show predominantly extensional earthquakes at the subduction zone outer rise, although compressional outer rise earthquakes occur at some subduction zones [*Stauder*, 1968; *Chapple and Forsyth*, 1979; *Christensen and Ruff*, 1988; *Kao and Chen*, 1996]. *Christensen and Ruff* [1988] proposed that, in addition to plate bending, stress along the megathrust during periods of interface locking affects stress distribution within the bending plate seaward of the subduction trench and that patterns of seismicity in the outer rise reveal the degree of coupling along the plate interface. Yet this relationship is still uncertain, as recent megathrust and outer rise earthquakes at some subduction zones have exhibited a more complicated pattern [*Ammon et al*., 2008; *Lay et al*., 2009; *Raeesi and Atakan*, 2009; *Lay et al*., 2010].

Outer rise earthquakes impact the hydration of oceanic plates prior to subduction. The pervasive faulting at the outer rise offshore from Nicaragua implies a clear pathway by which water can enter into the lower crust and uppermost mantle of the plate [*Ranero et al*., 2003], but the process by which water is pulled to depth

Table 1. Previously Studied Mariana Outer Rise Earthquakes

Date	Latitude	Longitude	Depth[a]	Type of Event	Magnitude	Reference
17 Jan 1940	17.24	148.12	n/a	Strike-slip[b]	*M* 7.3	[*Okal et al*., 2013]
14 Jun 1942	14.53	147.92	n/a	Compression[b]	*M* 7.0	[*Okal et al*., 2013]
4 July 1964	11.72	144.63	n/a	Tension	*Mb* 6.0	[*Katsumata and Sykes*, 1969]
27 Oct 1966	22.15	145.94	n/a	Tension	*Mb* 6.0	[*Katsumata and Sykes*, 1969; *Okal et al*., 2013]
5 Apr 1967	20.00	147.35	n/a	Tension	*Mb* 5.9	[*Katsumata and Sykes*, 1969]
1 Sept 1970	17.7	147.6	n/a	Tension	*Mb* 6.3	[*Chapple and Forsyth*, 1979; *Okal et al*., 2013]
11 May 1974	19.7	147.3	n/a	Tension	*Mb* 6.4	[*Chapple and Forsyth*, 1979; *Okal et al*., 2013]
5 Apr 1990	15.288	147.397	16	Tension	*Ms* 7.5	[*Yoshida et al*., 1992]
5 Apr 1990	15.125	147.596	23 ± 5	Tension	*Mw* 7.5	[*Zhang and Lay*, 1992]

[a]Depth determined through waveform modeling.
[b]Earthquake focal mechanism determined by limited historic records.

despite high lithostatic pressure is uncertain. *Faccenda et al*. [2009] postulate that tectonic pressure gradients within the upper oceanic lithosphere created by plate bending pulls water deep into the plate mantle, and this process could be further enhanced by other proposed mechanisms, such as seismic pumping through faults [*Sibson*, 1994], thermal cracking [*Korenaga*, 2007], or migrating fluid-filled cracks (vug waves) [*Phipps Morgan and Holtzman*, 2005]. Although the water transport mechanism is uncertain, recent seismic studies provide evidence that the oceanic mantle is significantly altered by serpentinization [*Contreras-Reyes et al*., 2007; *Ivandic et al*., 2010; *Van Avendonk et al*., 2011; *Savage*, 2012].

If serpentinization of mantle minerals occurs along all outer rise faults, then significantly larger amounts of water could be stored within plates prior to subduction [*Ranero et al*., 2003] causing an underestimate in the total amount of subduction zone water inputs. The amount of hydration within the different layers of the subducting oceanic plate has important effects on the progression of slab dehydration with depth [*Jarrard*, 2003; *Hacker*, 2008]. At intermediate depths, water is expelled from the lower crustal layers and, depending on the initial conditions of the subducting plate, possibly also from upper mantle serpentinites; this impacts volcanic arc and back-arc basin outputs [*Gill*, 1981; *Jarrard*, 2003; *Kelley et al*., 2006; *Van Keken et al*., 2011].

Water released at intermediate depths may travel to other parts of the slab, enabling intermediate and deep earthquakes or reacting with other slab minerals to form high-pressure hydrous phases, which are stable to greater depth [*Raleigh and Paterson*, 1965; *Meade and Jeanloz*, 1991; *Ulmer and Trommsdorf*, 1995; *Schmidt and Poli*, 1998]. Depending on the conditions of the plate and rate of subduction, at deeper depths mantle serpentinites, in particular, antigorite should carry water into the mantle deeper than the subduction zone mantle wedge [*Rüpke et al*., 2004; *Hacker*, 2008; *Van Keken et al*., 2011]. Deep transport of water is suspected to occur at subduction zones where the subducting slab is very old (cold) and converging rapidly [*Van Keken et al*., 2011]; such numerical models are reinforced by observations from the Tongan subduction zone indicating a low-velocity region within the slab, likely related to serpentinite [*Savage*, 2012].

2.2. Faulting and the Water Cycle at the Mariana Subduction Zone

Mariana outer rise bathymetry exhibits distinct faults, located closer than 100 km distance from the trench, with an onset at approximately the 6000 m bathymetric depth contour [*Oakley et al*., 2008; *Gardner*, 2010]. *Oakley et al*. [2008] found that seafloor fabric is reactivated where it forms an angle less than ~25° with the Mariana trench axis. When this angle is greater than ~25°, small offsets occur on existing faults, but the largest offsets occur on newly created, trench-parallel faults [*Oakley et al*., 2008]. Results from MCS surveys at the Mariana Trench do not resolve the maximum depth extent of outer rise faults [*Oakley et al*., 2008]; however, near-surface offsets indicate that fault throws change significantly along strike and are impacted by the angle of the incoming seafloor fabric with the subduction trench, the depth of the subduction trench, and the presence of seafloor seamounts on the incoming Pacific plate. Results from *Oakley et al*. [2008] also indicate that the inclination of the Pacific plate changes abruptly at the Central Mariana trench axis—from ~1–2° seaward of the trench axis to ~8–9° landward of the trench, beneath the fore arc. They interpret this abrupt change as evidence that the Pacific plate fails completely, rather than bends, as it subducts [*Oakley et al*., 2008].

At the Mariana subduction zone, few outer rise earthquakes have been studied to date; results for prior research of Mariana outer rise earthquakes are compiled in Table 1. Very few of these events have had depths

determined through waveform inversion techniques; rather most have been studied through earthquake relocation methods. Directly beneath the Mariana trench axis, a large, *Mw* 7.5 extensional earthquake occurred on 5 April 1990 and created a minor tsunami [*Zhang and Lay*, 1992; *Satake et al*., 1992; *Yoshida et al*., 1992]. The source of this earthquake was studied extensively by both *Zhang and Lay* [1992] and *Yoshida et al*. [1992]. *Zhang and Lay* [1992] estimate a depth of 23 ± 5 km centroid depth on a steep westward dipping fault plane, whereas *Yoshida et al*. [1992] find a depth of 16 km on a moderate westward dipping fault plane. Based on relocation of aftershocks, *Yoshida et al*. [1992] propose that the fault was ~40 km wide; however, significant error should be expected when using aftershock locations to infer the dimensions of a fault. The occurrence of such a large, extensional outer rise earthquake suggests that the Pacific plate is experiencing large extensional forces; combined with the large-offset faulting observed from seafloor bathymetry, the minerals within the oceanic plate mantle have the potential to be significantly hydrated, although the depth extent of hydration is yet unknown.

Due to the presence of a number of well-exposed serpentinite seamounts located along the length of the Mariana fore arc [*Fryer et al*., 1999], it is often expected that water plays an important role in the processes occurring at the Mariana subduction zone. Results from the MARGINS Mariana SubFac Seismic Experiment indicate that the shallow mantle wedge beneath the Mariana fore arc is serpentinized [*Tibi et al*., 2008; *Pozgay et al*., 2009; *Barklage*, 2010; *Pyle et al*., 2010]. The water contents of volcanic arc and back-arc outputs have been found to vary along the length of the margin, exhibiting no clear patterns of hydration along strike [*Kelley et al*., 2006; *Shaw et al*., 2008; *Kelley et al*., 2010; *Parman et al*., 2011]. Back-arc magmas at Mariana generally are ~0.5 wt % water, and island arc magmas range from ~2–6 wt % water [*Kelley et al*., 2006; *Shaw et al*., 2008; *Kelley et al*., 2010; *Parman et al*., 2011]. At Southern Mariana, the back arc is separated from island arc volcanoes by only 20–30 km, and back-arc volcanics in the region exhibit similarities to volcanic arc outputs, including increased concentration of water [*Fryer et al*., 1998; *Martinez et al*., 2000; *Taylor and Martinez*, 2003, and references therein]. At the southernmost boundary, the upper Philippine Plate is rifting directly over the subducting slab, and *Martinez et al*. [2012] propose that the water-rich setting promotes a weakened overriding oceanic lithosphere characterized by broad rifts and diffuse volcanism. Despite the indications of large amounts of shallow and intermediate depth water flux, only small amounts of water are thought to be carried deeper, beyond the mantle wedge [*Van Keken et al*., 2011]. However, this result is dependent upon the estimated amount of slab mantle serpentinization, which is in fact unconstrained for most subduction zones, including the Mariana subduction zone [*Van Keken et al*., 2011].

3. Data and Methods

3.1. Earthquake Relocation

Prior to waveform inversion, earthquakes were relocated to delineate events within the subducting plate near the trench from those in the shallow thrust zone in the fore arc. In general, shallow thrust earthquakes in the Mariana subduction zone do not occur within about 60 km of the trench axis [*Emry et al*., 2011]. Earthquake arrival time data were collected from the *International Seismological Centre On-line Bulletin* [2010] for all Global Centroid Moment Tensor (GCMT) earthquakes occurring between 9–26°N and 138–154°E from 1 January 1976 to 1 October 2010 [*Dziewonski et al*., 1981; *Ekström et al*., 2012]. All GCMT earthquakes seaward of the trench axis plus all events within 80 km landward of the trench axis were then split into four regions and relocated in two- and in three-dimensional space; the lateral positions of the two- and three-dimensional results are very similar. Four separate regions were used in the relative relocation to ensure that all earthquakes in the region are sampling similar global velocity heterogeneity. These regions were distinguished by latitude: the southern region near Guam extended from 10 to 14.5°N; the central region, near Celestial seamount extended from 14.5 to 17.5°N; the region near Big Blue seamount extended from 17.5 to 20.5°N; the northernmost region, north of Maug and almost into the Bonin subduction zone extended from 20.5 to 24°N (Figure 1).

The relative relocations were carried out using the hypocentroidal decomposition algorithm [*Jordan and Sverdrup*, 1981]. Initial locations were taken from the ISC, and travel times for P, pP, PKP, and *S* phases from each event were calculated according to the IASP91 Earth Model [*Kennett and Engdahl*, 1991]. *S* phases were used only for stations closer than 20° to the earthquake hypocenter due to large errors frequently found for teleseismic *S* wave arrival times reported to the ISC. The number of earthquakes relocated for each region varied greatly due to the difference in number of GCMT events occurring since 1976. In Southern Mariana

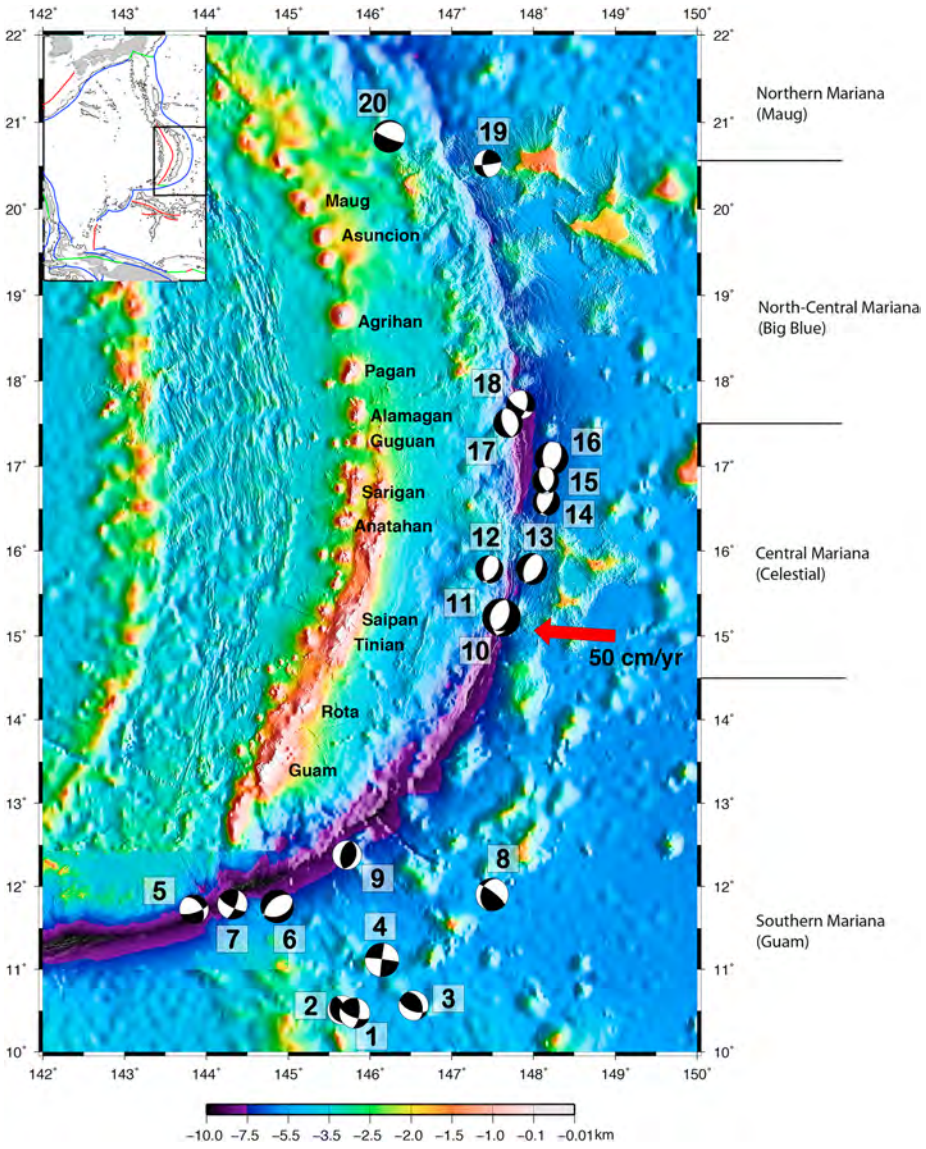

Figure 1. Relocated GCMT earthquakes in map view. Lower hemisphere stereographic projections for earthquakes are shown with compressional *P* wave quadrants (containing the *T* axis in black) and dilatational *P* wave quadrants (containing the *P* axis in white). The event numbers next to each focal mechanism correspond to Tables 2 and 4. The red arrow shows the angle of convergence of the Pacific plate relative to the Mariana fore arc as determined by *Kato et al*. [2003]. High-resolution bathymetry data in Northern and Central Mariana are from 2010 Mariana Law of the Sea Cruise [*Gardner*, 2010] and high-resolution bathymetry data in Southern Mariana are courtesy of F.Martinez. The color scale for bathymetry is positioned below and is the same for all bathymetric maps in the paper. (inset) Tectonic setting of the Philippine Sea. Bathymetry contours are shown by thin black lines. Subduction trenches are shown in blue; spreading centers are shown in red; transforms are shown in green.

near Guam, 151 events were relocated; 42 events were relocated in the central region east of Celestial Seamount; 28 events were relocated in the central region east of Big Blue Seamount; and 16 events were relocated in the northernmost region, north of Maug.

3.2. Earthquake Source Inversion From *P* and *SH* Waveforms

Following relocation, we requested waveform data from the IRIS Data Management Center (DMC) for all GCMT earthquakes greater than or equal to *Mw* 5.0 occurring seaward of the trench or in close proximity to the trench. For all earthquakes except one, only broadband data were used. For one earthquake occurring in 1990 (Event 11, Table 2), a combination of broadband and long-period (1 sps) data was inverted due to a limited number of good

Table 2. Mariana Earthquakes With Depths Obtained by Waveform Inversion (Ordered by Increasing Latitude)

Event	Date	Time (UTC)	Latitude (°N)	Longitude (°E)	Depth[ab] (km)	Time Func. (sec)	*Mw*	Type of Event[c]	# *P* Data	# *SH* Data	Top Freq. (Hz)	Misfit[d]
1	12 Nov 2007	00:25:45.76	10.4706	145.8160	5 ± 1	1	5.73	SS	23	19	0.5	0.4649
2	30 Sept 2007	15:02:18.09	10.5057	145.6567	7 ± 1	3	5.53	C	21	13	0.5	0.4019
3	31 Aug 2003	09:01:32.43	10.5619	146.5327	34 ± 2	1	5.54	C-SS	23	11	0.5	0.3149
4	10 July 2010	11:43:35.44	11.1146	146.1478	12 ± 1	2	6.32	SS	24	21	0.5	0.4707
5	4 May 2005	04:38:09.54	11.7264	143.8479	11 ± 1	1	5.43	SS	12	7	0.5	0.3620
6	19 Dec 2000	13:11:49.37	11.7616	144.8650	12 ± 2	7	6.23	T	25	11	0.5	0.4438
7	13 May 2004	17:34:36.88	11.7851	144.3199	24 ± 1	2	5.63	SS	19	16	0.2	0.3117
8	2 Apr 2001	06:50:04.93	11.9032	147.4938	31 ± 2	3	5.49	SS	12	22	0.5	0.2585
9	10 Nov 1997	19:04:23.69	12.3763	145.7198	34 ± 3	1	5.43	C	28	22	0.2	0.4963
10	5 Apr 1990	21:12:37.95	15.2195	147.6103	18 ± 2	5	7.21	T	9	11	0.5	0.2486
11	6 Apr 1990	14:57:21.23	15.2550	147.5977	13 ± 1	6	6.15	T	11	11	0.18	0.2799
12	4 Aug 2001	18:55:11.22	15.7843	147.4597	18 ± 1	3	5.20	T	6	8	0.18	0.3832
13	13 Oct 1990	00:20:22.19	15.7884	147.9803	8 ± 4	4	5.89	T	9	6	0.5	0.5212
14	10 Nov 1995	22:30:59.80	16.5791	148.1561	13 ± 3	1	5.17	T	12	2	0.2	0.3479
15	16 July 2008	17:23:44.20	16.8317	148.1483	9 ± 3	1	5.04	T-SS	7	8	0.18	0.4267
16	30 Aug 1998	01:48:09.84	17.0937	148.2210	10 ± 1	5	6.31	T	23	17	0.5	0.2796
17	4 May 2000	23:24:41.34	17.5084	147.6909	11 ± 2	1	5.52	T	11	14	0.5	0.2894
18	1 May 2003	00:14:09.47	17.7258	147.8452	9 ± 1	1	5.38	SS	17	9	0.2	0.3186
19	19 July 2000	14:28:38.97	20.5277	147.4411	25 ± 1	2	5.20	SS	4	5	0.2	0.3700
20	14 Feb 2006	15:27:24.95	20.8419	146.2316	49 ± 2	4	6.17	T	32	18	0.5	0.5338

[a]Denotes depth beneath seafloor (depth within plate).
[b]Depth error calculated as depth where the misfit is 5% more than the best fitting solution, not including errors in velocity model.
[c]SS, strike-slip; C, compression; T, extension.
[d]Misfit is calculated according to equations (1) and (2).

broadband waveforms for that event. Events prior to 1990 had no clear broadband waveforms and on average only ~5–10 clear long-period waveforms, and so the events were not investigated further.

We inverted teleseismic *P* and *SH* waveforms from stations at distances of 30–90° to determine the best fitting source parameters for earthquakes located on the incoming plate or near the trench axis. For two earthquakes with fewer high-quality arrivals, we searched through waveforms at 20–30° and 90–100° in order to collect more data (Table 2; Events 13 and 15). With the expanded distance range, we found only a few more clear waveforms (five or less) to add to the inversions, and it should be noted that the resulting depths of these events are not as well constrained as for others in the set due to the limited number of high-quality waveforms (Table 2). Waveforms were visually inspected for quality signals at frequencies of 0.02–0.5 Hz. For some events, low-frequency (0.02–0.18 Hz or 0.02–0.2 Hz) waveforms were sufficiently clear but the higher frequencies up to 0.5 Hz were not, due to the microseism peak around 0.2 Hz. For the one event in 1990 that utilizes long-period (1 sps) data, the upper frequency stop band was set at 0.18 Hz. The instrument responses provided by the IRIS DMC for each station were deconvolved from the data prior to comparison with the synthetics.

Waveform synthetics were computed using ray theory [e.g., *Langston and Helmberger*, 1975] and utilized the ray parameter corresponding to teleseismic propagation in an IASP91 velocity model. Synthetics were calculated for three fundamental double-couple source geometries and then linearly combined to obtain synthetics for each focal mechanism in the grid search. A ray expander routine was used to compute all the reflections and conversions in the near-source structure model above a cut-off amplitude, and the source time function was modeled as a half sine wave with a best fitting duration determined by the inversion. We found our best fitting source depth, time function, and focal mechanism strike, dip, and slip using a grid search (e.g., Figure 2). In the grid search, misfit was calculated at each station as the squared amplitude misfit between data and synthetics normalized over the squared amplitude of the data, multiplied by the weight assigned to that station:

$$\text{Misfit} = \frac{\sum_{i=n_1}^{n_2} \left(d(i) - s(i) \times M\right)^2}{\sum_{i=n_1}^{n_2} d(i)^2} \quad (1)$$

where i spans the time window for which misfit is to be calculated, n_1 is the starting time for the window, n_2 is the end time for the window, d is each data point, s is each synthetic value, and M is the median seismic moment

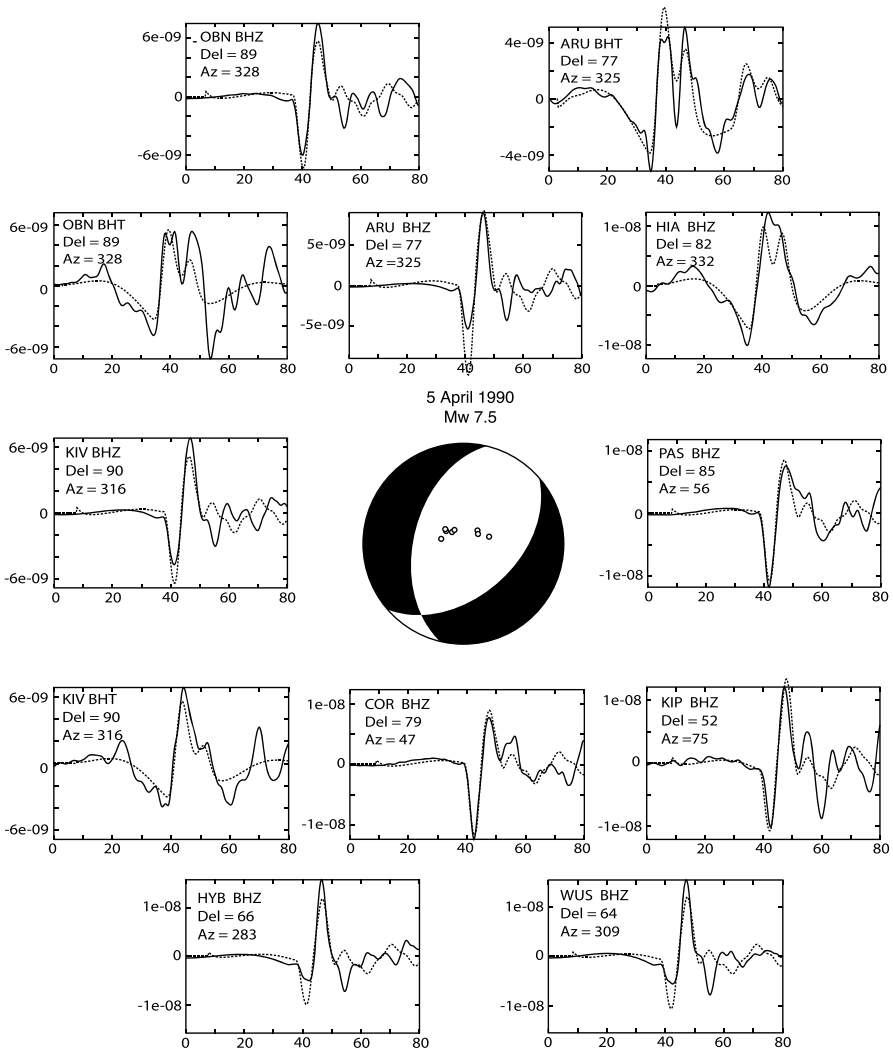

Figure 2. The best fit focal mechanism for the 5 April 1990 earthquake at 18 km depth in the Pacific plate. First-motion polarities for *P* wave arrivals are indicated by open circles (dilatation) and closed circles (compression). Select waveform data (BHZ and BHT) are shown as thick black lines and best fit synthetic waveforms are shown as dashed black lines. The *x* axis (time) is given in seconds and the *y* axis (displacement amplitude) is in meters. Distance (Del) and azimuth (Az) are in degrees.

found for the whole set of stations. Total misfit for each mechanism, depth, and time function combination was the summation of individual station misfits (1) over the summation of weights assigned to each station:

$$\text{SolutionMisfit} = \frac{\Sigma_{i=1}^{n}\text{Misfit}(i)}{\Sigma_{i=1}^{n}\text{Weight}(i)} \tag{2}$$

where n is the number of stations used in the inversion.

The source-side velocity models used in the waveform inversion differed along strike, based on the MCS reflection results from *Oakley et al.* [2008]. Table 3 presents the latitude ranges and the velocities and thicknesses of the water, sediments (where applicable), upper crustal, lower crustal, and mantle layers. Although the thicknesses of the layers changed along strike, the seismic velocities and densities remained constant for each layer and are listed within Table 3. Effects from imperfectly known source-side velocity models are discussed in further sections and in the supporting information.

Synthetic waveform fits to the data are shown in Figure 2 for the large 5 April 1990 event. The good waveform match indicates that the timing of the depth phases (pP and sP for *P* waves and sS for *SH* waves), which is the waveform feature most dependent upon source depth are well fit, and the depth is well determined. The

Table 3. Velocity Models Used During Inversion

		Velocity Models			
Layer	Properties	Northern Mariana (20–21°N)	Central Mariana (17.5–18°N)	Central Mariana (15–17°N)	Southern Mariana (10–13°N)
Water	$\alpha = 1.5$ km/s $\beta = 0$ km/s $\rho = 1.0$ g/cm^3	Thickness: 5–6 km	Thickness: 6–8 km	Thickness: 4–6 km	Thickness: 4–8 km
Sediment	$\alpha = 2.0$ km/s $\beta = 1.1$ km/s $\rho = 2.0$ g/cm^3	Thickness: 0 km	Thickness: 0–1 km	Thickness: 0 km	Thickness: 0 km
Upper crust	$\alpha = 5.2$ km/s $\beta = 3.0$ km/s $\rho = 2.6$ g/cm^3	Thickness: 2 km	Thickness: 2 km	Thickness: 3 km	Thickness: 3 km
Lower crust	$\alpha = 6.8$ km/s $\beta = 4.0$ km/s $\rho = 3.0$ g/cm^3	Thickness: 3 km	Thickness: 3 km	Thickness: 4 km	Thickness: 4 km
Mantle	$\alpha = 8.0$ km/s $\beta = 4.5$ km/s $\rho = 3.3$ g/cm^3	N/A	N/A	N/A	N/A

waveform inversion treats the earthquake as a point source and solves for the centroid depth of the event, or rather the average depth of moment release and cannot be used to determine the spatial dimensions of the fault. For large earthquakes, such as the 5 April 1990 *Mw* 7.5, the fault dimensions extend shallower and deeper than the centroid depth. Depending on the amount of slip during the event and the shape of the rupture area, the fault likely extends an additional 10–20 km deeper than our centroid depth for an event of this size [*Kanamori and Anderson*, 1975]. The rest of the events are much smaller than the 5 April 1990 event, and so the fault size will be much smaller. For these events, the centroid depth will be within ~3–10 km of the maximum faulting depth.

Initially, the search was performed over the entire model space with larger source parameter increments, and then searched again near the best fitting solutions with a smaller increment to obtain the optimal fit to the data within 1 km of depth, 1 s in source duration, and 1° of strike, dip, and slip respectively. The depth search extended throughout the oceanic crust and into the mantle to a depth 45 km below the seafloor. Figure 3 shows an example of solution misfit within the depth and source time function parameter space for the large extensional event in 1990, corresponding to Figure 2 (Table 2, Event 10). Although less data are available during the early 1990s, the contours demonstrate that there is only one minimum within the depth-source time parameter space. Similar plots for each earthquake are located in the supporting information (Figures S1–S19), measures of waveform fits to the data are provided in Table 2, and other contributions to errors in depth are reviewed in section 5 and in the supporting information.

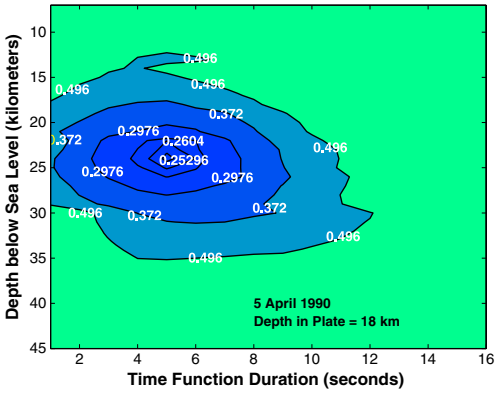

Figure 3. Misfit contours in depth versus source time function parameter space for 5 April 1990 large, extensional outer rise earthquake (Event 10, Table 2). Misfit is calculated using equations (1) and (2). Contours for the solutions at 2%, 5%, 10%, 20%, and 50% greater than the best fit solution are given. The *y* axis shows depth (kilometers) below sea level. The *x* axis represents the source time function (seconds).

One earthquake (Event 14, Table 4) showed clear *P* wave arrivals at some stations but had insufficient high-quality waveforms to provide a well-constrained focal mechanism. In this instance, the best fitting GCMT double-couple focal mechanism was used and only the best fitting depth and time function were determined. We expect that focal mechanisms were robustly constrained by the GCMT solutions; therefore, agreement between the fault parameters for the GCMT solutions and for our focal mechanism inversions provides added confidence in the stability of the waveform inversions. Table 4 lists

Table 4. Best Fitting Focal Mechanism From Waveform Inversion and the Corresponding GCMT Double-Couple Solution

Event #	Strike (deg)	Dip (deg)	Slip (deg)	Moment (N m)	Depth (km)	GCMT Strike (deg)	GCMT Dip (deg)	GCMT Slip (deg)	GCMT Moment (N m)	GCMT Depth (km)
1	8	66	154	4.99E17	5	12	60	146	4.74E17	12
2	142	24	76	2.49E17	7	140	33	68	1.96E17	12
3	111	58	61	2.56E17	34	116	64	67	2.21E17	31
4	277	86	1	3.75E18	12	99	77	8	3.17E18	13.7
5	319	43	−29	1.77E17	11	309	50	−25	1.34E17	12
6	68	41	−76	2.76E18	12	72	34	−80	1.93E18	15
7	22	72	164	3.55E17	24	27	83	178	4.95E17	28.2
8	197	32	156	2.19E17	31	180	24	138	2.43E17	40.5
9	20	37	97	1.79E17	34	4	27	82	1.83E17	42.9
10	189	45	−98	8.18E19	18	185	31	−108	1.63E20	15
11	18	49	−94	2.08E18	13	35	32	−50	2.33E18	15
12	185	52	−109	7.81E16	18	195	55	−67	4.74E16	41
13	36	42	−77	8.71E17	8	30	24	−85	7.52E17	15
14[a]	172	32	−123	7.25E16	13	172	32	−123	6.29E16	17.1
15	18	40	−57	4.52E16	9	11	42	−82	4.17E16	17.1
16	26	48	−67	3.70E18	10	8	39	−80	3.41E18	16
17	350	32	−83	2.41E17	11	347	19	−116	2.26E17	15
18	12	54	−30	1.46E17	9	16	55	−17	1.76E17	15
19	177	57	7	7.82E16	25	168	83	0	6.14E16	53.7
20	113	80	−75	2.27E18	49	124	80	−64	3.03E18	41.2

[a]GCMT double-couple parameters were assumed due to lack in clear *S* phases in data.

differences in fault parameters, moment, and depth between our waveform inversion results and the GCMT best fitting double couple.

3.3. Flexure Modeling

We compare the earthquake centroid depth results with a theoretical distribution of stress within the bending Pacific plate to determine whether our predictions for depth and location of compression, extension, and the neutral plane match that predicted by the bathymetric profile of the bending oceanic plate seaward of the trench axis. In order to accomplish this, we use the tAo two-dimensional finite-difference flexure package of *Garcia-Castellanos et al.* [1997]. This method was initially created to study rheologic properties beneath foreland basins by linking crustal shortening, erosion, sedimentation, and lithospheric flexure [*Garcia-Castellanos et al.*, 1997]. However, the method can be applied to model other systems, such as oceanic plate flexure seaward of subduction thrust systems [*Garcia-Castellanos et al.*, 2000].

Rather than model oceanic plate flexure as a purely elastic or viscoelastic process, which does not reflect strength profiles inferred from experiments [*Goetze and Evans*, 1979], an elastic-plastic depth-dependent rheology is employed to provide a more realistic stress distribution with depth in the lithosphere [*Garcia-Castellanos et al.*, 1997]. This plate rheology allows for brittle failure to occur at shallow depths, limiting the amount of stress that the top of the plate can withstand [*Garcia-Castellanos et al.*, 1997]. The equations for frictional sliding are sensitive only to depth (pressure). The bottom of the plate is limited by the temperature-sensitive flow laws that govern ductile deformation in dry olivine. At low shear stress ($<$ 200 MPa) the flow law of olivine from *Goetze* [1978] and *Goetze and Evans* [1979] is assumed to control mantle deformation:

$$\dot{\varepsilon}_P = 70\sigma_s^3 \exp\frac{-Q_p}{RT} \tag{3}$$

Where $\dot{\varepsilon}_P$ represents the power law strain rate of deformation, σ_s is shear stress, Q_p is the power law activation energy for dry olivine, R is the universal gas constant, and T is the temperature (Table 5). At higher shear stress ($>$ 200 MPa), the Dorn law is used to describe mantle flow [*Goetze*, 1978; *Goetze and Evans*, 1979]:

$$\dot{\varepsilon}_D = 5.7 \times 10^7 \exp\left\{\frac{-Q_D}{RT}\left(1-\frac{\sigma_s}{\sigma_p}\right)^2\right\} \tag{4}$$

where $\dot{\varepsilon}_D$ represents the strain rate of deformation, σ_s is shear stress, σ_p is the Peierl's stress, Q_D is the Dorn activation energy for dry olivine, R is the universal gas constant, and T is temperature (Table S1).

Table 5. Scenarios for Water Inputs Into South Central Mariana (500 km length)

Scenario	Water Input Within Mantle Serpentinites (10^6 Tg/Myr)	Total Amount of Input Water (10^6 Tg/Myr)
No mantle serpentinite [*Van Keken et al.*, 2011]	0	7.35
2 wt % H_2O to 2 km [*Van Keken et al.*, 2011]	3.4	10.7
Fully serpentinized [*Van Keken et al.*, 2011]	14.8	22.1
2 wt% H_2O to 5 km	8.3	15.6
2 wt % H_2O to 11 km	18.2	25.5
3.5 wt % H_2O to 5 km	14.5	21.8
3.5 wt % H_2O to 11 km	31.8	39.1
3.5 wt % H_2O to 5 km; 1 wt% H_2O to 11 km	22.7	30
2 wt % H_2O to 5 km for 250 km; 2% to 11 km for 250 km	13.3	20.6
3.5 wt % H_2O to 5 km for 250 km; 3.5% to 11 km for 250 km	23.2	30.5
2 wt % H_2O to 11 km; tapering to 0 km at ends	5.5	12.8

In the tAo software, the moment and curvature are calculated iteratively from an initial elastic plate thickness following the methods of *McNutt* [1984] and *Waschbusch and Royden* [1992] and the depth-dependent yield stress envelope then limits stress within the bending plate [*Garcia-Castellanos et al.*, 2000]. The yield stress envelope is determined from the temperature distribution for oceanic lithosphere given a certain plate age. We use the temperature profile for a 150 Myr plate using the GDH1 cooling plate model of *Stein and Stein* [1992], which defines the thickness of the lithosphere as the depth to the 1450°C isotherm. The *Stein and Stein* [1992] thermal model predicts a thinner oceanic lithosphere (95 km) for older ($>$ 75 Myr) plates and better fits the trend of seafloor depth with age than prior thermal models [*Parsons and Sclater*, 1977]. Furthermore, *Garcia-Castellanos et al.* [2000] find that flexure profiles computed for the Tongan trench using GDH1 [*Stein and Stein*, 1992] provide a better fit to the data than the *Parsons and Sclater* [1977] model.

Bathymetry data were collected from global and local grids, obtained through the *U.S. Department of Commerce, National Oceanic and Atmospheric Administration, National Geophysical Data Center*, [2006] and recent Law of the Sea cruises [*Gardner*, 2010]. Unlike the approach used by *Garcia-Castellanos et al.* [2000] for the Tonga subduction trench, profiles extending seaward of the subduction trench were not averaged along the entire length of the margin. Rather, input profiles for flexure models were specifically selected along corridors where few seafloor seamounts exist. This approach gives a better representation of the actual form of the bending plate, because the resultant profiles are impacted less by the multiple, large, seafloor seamounts seaward of the Mariana trench [*Wessel*, 2001]. Furthermore, our approach takes into consideration that the slope of the outer trench changes significantly along the length of the Mariana subduction zone and allows us to explore how changes in the flexure of the plate along strike may be reflected in our earthquake locations and depths.

Using the trench-perpendicular bathymetry profiles (with seamounts avoided) as discussed above, we weigh most heavily the points closest to the trench (within 150 km from the trench) and the points farthest from the trench are weighted least (farther than 350 km from the trench). We run a grid search using the distance-weighted bathymetric profiles to determine an estimate for the best fitting applied parameters (moment and external forces) and to approximate the distance of maximum plate-bending moment and the vertical stress profile and failure criteria that corresponds to that distance.

4. Results

4.1. Earthquake Locations and Depths

We relocated and determined accurate depths for 20 earthquakes within the Pacific plate (Figure 1 and Table 2). Of these, 10 were normal-faulting events or normal-faulting events with some component of strike-slip motion, with the remaining 10 showing strike-slip or compressional mechanisms. The earthquakes that we interpret to be related to Pacific plate bending were located within 70 km landward or 40 km seaward of the trench axis. Five events with depths determined by waveform inversion were located at 150–225 km seaward from the trench axis and are compressional or strike-slip earthquakes with tensional (*T*) axes that are not oriented perpendicular to the trench axis. The overall trend of the Pacific plate-bending earthquakes changes from strike slip and obliquely striking extensional earthquakes in Northern Mariana to purely extensional outer rise earthquakes in North central Mariana to a combination of extensional, strike slip, and compressional mechanisms at Southern Mariana. Here we

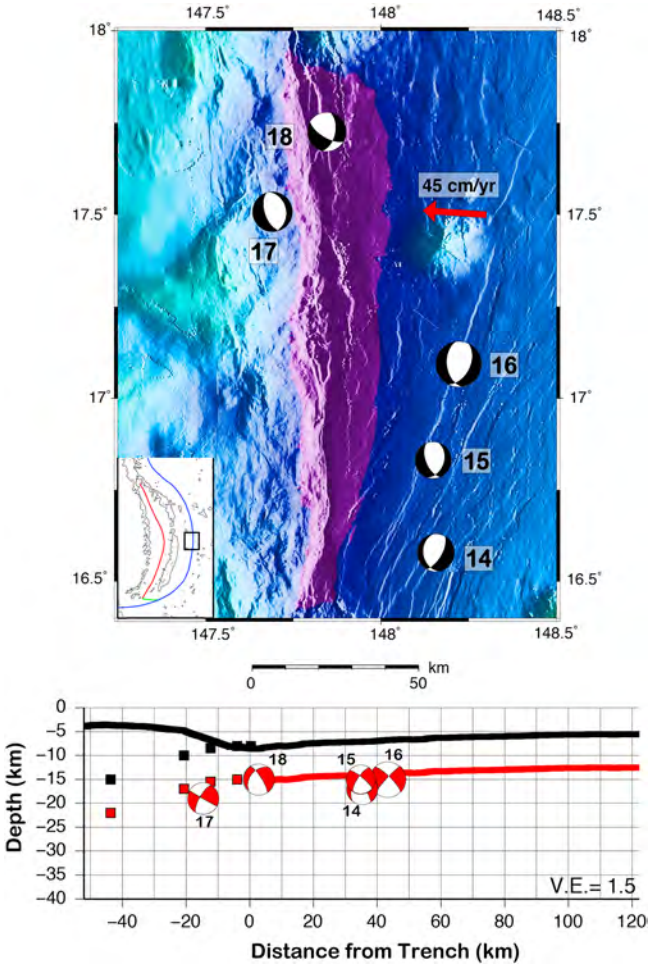

Figure 4. (top) Relocated GCMT earthquake locations in mapview. Lower hemisphere stereographic projections for earthquakes are shown with compressional quadrants (in black) and dilatational quadrants (in white). Event numbers next to each focal mechanism correspond to Tables 2 and 4. The red arrow shows the angle and rate of Pacific plate convergence relative to the fore arc as determined by *Kato et al.* [2003]. High-resolution bathymetry data are from *Gardner* [2010]. The bathymetry scale is the same as in Figure 1. Inset shows the tectonic setting of the Mariana Islands. Bathymetry contours are shown by thin black lines. The trench axis is shown in blue; back-arc spreading center is in red; transform is in green. (bottom) Trench-perpendicular cross section with the location of the subduction trench at 0 km; negative distances indicate the distance landward (or west of the trench) and positive distances indicate seaward distances (or east of the trench). Thick black lines show the bathymetry along (17.25°N, 147.3577°E) to (17.2752°N, 148.9311°E). Thick red lines show depth to the Moho used in our waveform inversion. Black squares show the depth to the plate interface at ~17°N from *Oakley et al.* [2008]; red squares indicate the continuation of the Moho landward from the trench. Focal mechanisms for the region are rotated 90° into cross section. Dilatational quadrants are indicated by white while compressional quadrants are indicated by red. The event numbers next to each focal mechanism correspond to Tables 2 and 4. Vertical exaggeration (VE) is 1.5.

will concentrate the discussion on the Central and Southern regions where there are sufficient earthquakes to draw some conclusions.

4.1.1. Central Mariana

In Central Mariana from 15 to 18°N, no compressional GCMT earthquakes were identified in the trench or outer rise but many extensional earthquakes with strikes parallel to the trend of the trench axis occurred. A more detailed view of the bathymetry and locations of the earthquake results in the highly faulted region from 16.4 to 18°N is shown in Figure 4. The depths of the five earthquakes in this region range from 9–13 km beneath the seafloor and are located within the top 6 km of the Pacific plate mantle. The earthquakes occurring seaward of the trench axis are located below several long faults exposed at the surface of the seafloor. The earthquake locations span an area from 20 km landward of the trench axis to 40 km seaward of the trench axis. Here unlike the region to the south where the large *Mw* 7.5 earthquake occurred, the surface of the Pacific plate is relatively devoid of seamounts and the depths of extensional earthquakes are shallower, extending only a few kilometers beneath the base of the crust.

A magnified view of the bathymetry and locations of inverted GCMT earthquakes in the vicinity (15–16°N) of the large 5 April 1990 outer rise earthquake is shown in Figures 5 and 6. The large extensional 5 April 1990 mainshock (Table 2, Event 10) was the deepest in our set of events; we determined a centroid depth of 24 ± 2 km (18 km beneath the seafloor) and a moment magnitude (*Mw*) of 7.21. In comparison, results from *Zhang and Lay* [1992] and *Yoshida et al.* [1992] for the same earthquake give a depth of 23 ± 5 km (*Mw* 7.5) and 16 km (*Mw* 7.5), respectively, by using the method of *Kikuchi and Kanamori* [1991]. As discussed, the large size of this earthquake requires faulting over a substantial depth range, suggesting that faulting extend to at least ~30–35 km below the seafloor (~23–28 km below the Moho). Figure 6 indicates that the 1990 earthquake likely faulted to the surface and is associated with the fault scarp found at the trench axis. Two of the three other earthquakes in this region occurred in 1990 and are aftershocks of this large earthquake (Table 2, Events 13 and 11). One small magnitude extensional

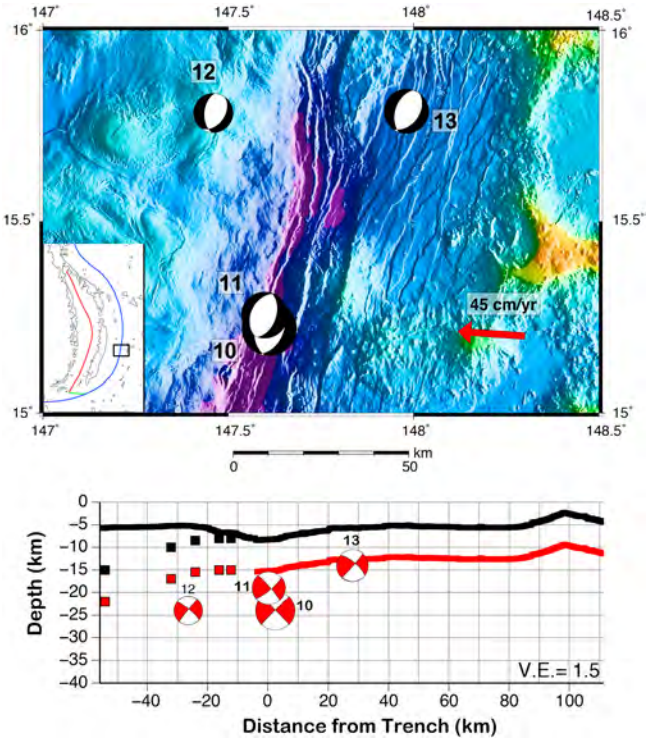

Figure 5. (top) Relocated GCMT earthquake locations in map view. Lower hemisphere stereographic projections are shown with compressional quadrants (in black) and dilatational quadrants (in white). Event numbers next to each focal mechanism correspond to Tables 2 and 4. The red arrow shows the angle of convergence of the Pacific plate relative to the Mariana fore arc as determined by *Kato et al*. [2003]. High-resolution bathymetry data are from *Gardner* [2010]. The bathymetry scale is the same as in Figure 1. (inset) Bathymetry contours are shown as thin black lines. The trench axis is in blue; back-arc spreading center is in red; transform faults are in green. (bottom) Trench-perpendicular cross section with the location of the trench axis at 0 km; negative numbers indicate the distance landward and positive values indicate seaward distances. Thick black lines show the bathymetry along (15.2236°N, 147.0582°E) to (14.9072°N, 148.5767°E). Thick red lines show depth to the Moho used in our waveform inversion. Black squares show the depth to the plate interface at ~17°N from *Oakley et al.* [2008]; red squares indicate the continuation of the Moho landward from the trench. Focal mechanisms for the region are rotated 90° into cross section. Dilatational quadrants are indicated by white while compressional quadrants are indicated by red. The event numbers next to each focal mechanism correspond to Tables 2 and 4. Vertical exaggeration (VE) is 1.5.

earthquake occurred during 2001 within the Pacific plate beneath the fore arc (Table 2, Event 12). The studied earthquakes in this region, located between 25 km landward (west) of the trench axis and 30 km seaward (east) of the trench axis, have depths ranging from 8 to 18 km beneath the top of the slab, down to a maximum depth of ~11 km below the Moho.

4.1.2. Southern Mariana

In comparison to Central Mariana, Southern Mariana has had few moderate to large extensional earthquakes (Figure 7). The extensional GCMT earthquakes large enough to be inverted are located near the southern Mariana Trench axis at depths of 12 km or less within the Pacific plate (Table 2, Events 5 and 6), and one moderate-sized compressional earthquake with a strike subparallel to the strike of the trench axis was located slightly north along the trench. The best fitting depth for this event is 34 km beneath the top of the Pacific plate (Table 2, Event 9). The orientations for these extensional and compressional earthquakes are consistent with what is expected given Pacific plate bending at the subduction trench. The locations of the earthquakes range from 20 km landward of the trench to 20 km seaward of the trench. A number of compressional and strike-slip earthquakes oriented at angles that are oblique to the strike of the trench axis were located at >150 km distance from the trench. The GCMT earthquakes for which we determine new depths in this location range in magnitude *Mw* (5.5–6.3) and in depth (5–34 km).

4.2. Flexure Models

The best fitting model for the bathymetric profile extending seaward of the trench axis at Southern Mariana indicates large amounts of plate flexure and regional compressive stresses (Figure 8). According to this result, the greatest amount of compression occurs within ~100 km of the trench axis at ~30–40 km beneath the surface of the Pacific plate. In this region, extension is predicted within 150 km distance from the trench, and at the point of maximum bending moment, the neutral plane is predicted to be ~20 km beneath the top of the plate, with brittle extensional faulting occurring down to ~15 km (Figure 9). The stress distribution predicted by this lowest misfit model matches the best with seismic constraints, in comparison to other low-misfit solutions, given the shallow extensional event and the compressional outer rise event at 34 km near the trench axis (Table 2, Event 9 and Figure S20).

At Central Mariana (17–18°N), the flexure model which best fits the Pacific plate bathymetry seaward of the trench axis predicts small horizontal compressional stresses and a small region of shallow extensional stresses

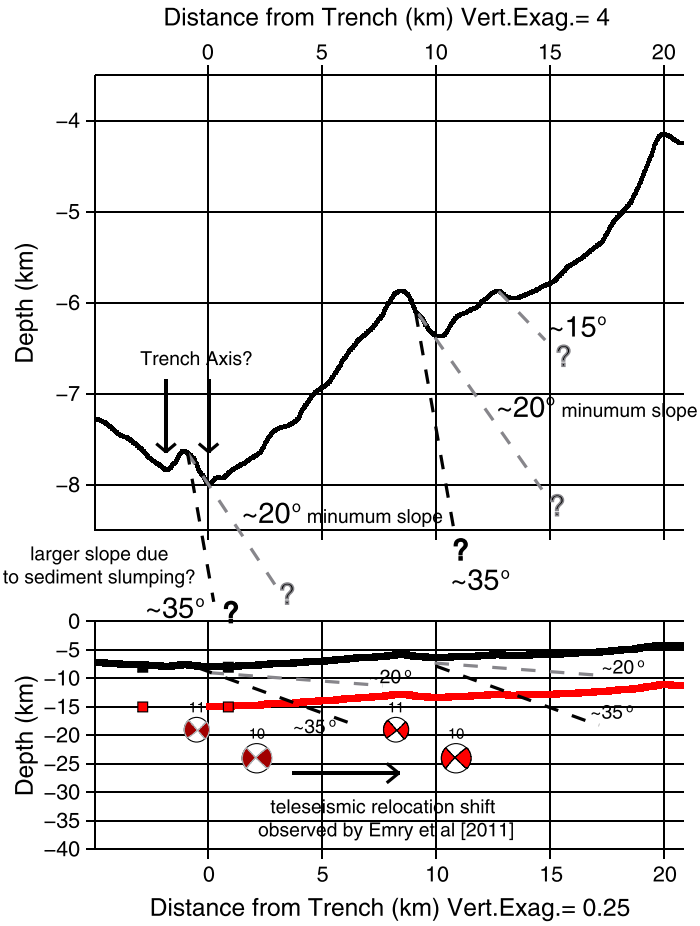

Figure 6. (top) Cross-sectional profile around the 5 April 1990 outer rise earthquake; vertical exaggeration (VE) = 4 along (15.4°N, 147.4°E) to (15.2°N, 148°E). Bathymetry is shown as thick black lines, estimated continuation of surface faults for dip measured from bathymetry (~15–20°) (gray dashed line) and for steeper-dipping faults (~35°) (black dashed line). (bottom) Same as above with vertical exaggeration (VE) = 0.25. Thick black lines indicate bathymetry; thick red line shows depth to Moho assumed by our waveform inversion technique. Black squares indicate depth to plate interface ~17°N as determined by *Oakley et al*. [2008]; red squares show continuation of the Moho landward from the trench. Focal mechanisms for the 5 April 1990 and 6 April 1990 earthquakes (Events 10 and 14, Table 4) are rotated 90° into cross section. *Emry et al*. [2011] compared local and teleseismic earthquake locations near the Mariana trench and found teleseismic locations shifted westward, so we applied a similar shift here to reduce the effects of global structure bias. Focal mechanisms at original relocation position are further west on the diagram; dilatational quadrants are indicated by white, and compressional quadrants are shown in maroon. Focal mechanisms with corrected positions are further east on diagram; dilatational quadrants are indicated by white, and compressional quadrants are indicated by red. Shallow-dipping faults are shown as dashed gray lines and steeper-dipping faults are shown as black dashed lines.

extending outward ~200 km from the trench axis (Figures 8 and 10). The predicted maximum extensional stresses within this region for the model are notably small, with a neutral plane depth of ~25 km at the point of maximum plate bending. This model predicts that brittle extensional faulting would cease at a depth of ~18 km. However, the centroid depth of the large 1990 extensional earthquake in our data set was 18 km, indicating that brittle extensional faulting extends to greater depths. Results from *Oakley et al*. [2008] using MCS reflection in this region show that the surface of the Pacific plate changes abruptly at the trench from 1–2° east of the trench to 7–8° west of the trench. When the profile of the Central Mariana Pacific plate is extended to include the shallowest portion of the plate interface already subducted beneath the toe of the Mariana fore arc, the best fitting flexure model is significantly different and predicts large extensional forces throughout the entire length of the plate (Figure 10). The predicted neutral plane for this model is ~38 km and brittle faulting is predicted to continue down to 30 km into the plate. However, none of the flexure models produced are able to match the kink in the Pacific plate bathymetry/shallow plate interface as observed by *Oakley et al*. [2008] (Figure 10).

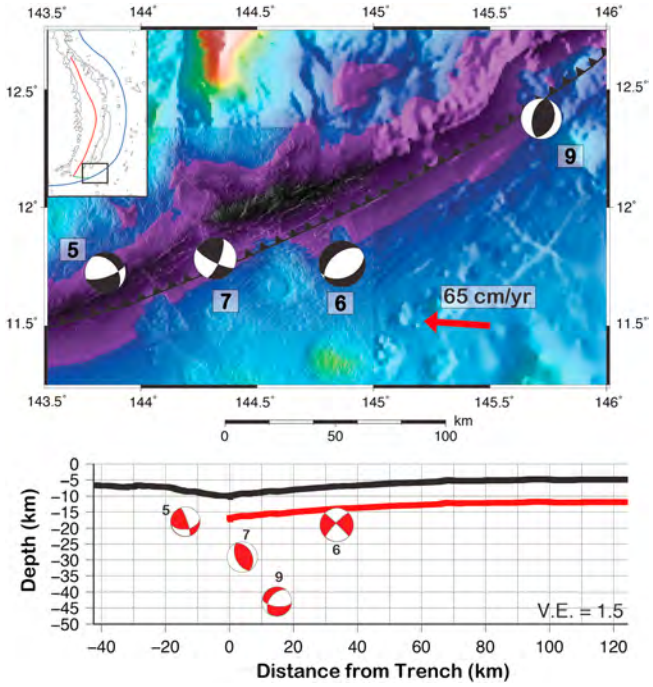

Figure 7. (top) Relocated GCMT earthquake locations from the Southern Mariana Trench in map view. Lower hemisphere stereographic projections for earthquakes have compressional quadrants (in black) and dilatational quadrants (in white). Event numbers next to focal mechanism correspond to Tables 2 and 4. Red arrow shows the angle and rate of Pacific plate convergence relative to the fore arc from *Kato et al.* [2003]. High-resolution bathymetry data are courtesy of F. Martinez. The bathymetry scale is the same as in Figure 1. Inset shows the tectonic setting of the Mariana Islands. Bathymetry contours are thin black lines. The subduction trench shown as a blue line; back-arc spreading center, red; transform boundary, green. (bottom) Trench-perpendicular cross section with the location of the subduction trench at 0 km; negative distances indicate the distance landward (or northwest of the trench) and positive distances indicate seaward distances (or southeast of the trench). Thick black lines show the bathymetry along (12.4708°N, 144.7513°E) to (11.1262°N, 145.4304°E). Thick red lines show depth to the Moho used in our waveform inversion. Black squares show the depth to the plate interface at ~17°N from *Oakley et al.* [2008]; red squares indicate the continuation of the Moho landward from the trench. Focal mechanisms for the region are rotated 90° into cross section. Dilatational quadrants are indicated by white while compressional quadrants are indicated by red. The event numbers next to each focal mechanism correspond to Tables 2 and 4. Vertical exaggeration (VE) is 1.5.

5. Discussion

5.1. Depth and Model Uncertainties

Our estimates of earthquake depth from waveform inversions are subject to our assumed seismic velocity structure near the earthquake source and the fit of synthetic waveforms to the data. To estimate the velocity structure, we used recent results from active-source seismic experiments throughout Mariana and Izu-Bonin (Table 2) [*Takahashi et al.*, 2007; *Oakley et al.*, 2008]. To estimate the depth uncertainty due to waveform misfit, we calculate "errors" as the difference in depth between the best fitting solution and those solutions with misfits 5% greater than the best (Table 2). Misfit contour plots for all earthquakes are provided in Figure 3 and the supporting information (Figures S1–S19). A more thorough discussion of depth uncertainties due to assumed velocity model and due to waveform misfit is given in the supporting information (Text S1).

The results of plate flexure models are nonunique; different combinations of external forces and bending moment in some instances produce similar theoretical profiles for the top of the plate (Figure S20). For both Southern and Northern Mariana, the greatest trade-off in modeled parameters occurred between the horizontal (regional) force and plate-bending moment. In addition to issues of nonuniqueness, uncertainty results from assumed model parameters, such as the material properties, rheological laws, and geotherms. A discussion of our assumptions is given in the supporting information (Text S2), and assumed model parameters are listed in Table S1.

5.2. Stress Distribution Within the Pacific Oceanic Plate at the Mariana Trench

The Pacific Plate at Central Mariana (15–18°N) has had many, recent, normal-faulting earthquakes. In this region, *Oakley et al.* [2008] observe that the incoming seafloor fabric is nearly parallel to the strike of the trench axis; south of ~16.5°N, preexiting faults are reactivated, but between ~16.5 and 18°N, new faults and reactivated faults exist together. The large 5 April 1990 *Mw* 7.5 extensional earthquake was located almost directly beneath the trench at significant depth within the mantle in this region [*Zhang and Lay*, 1992; *Yoshida et al.*, 1992] and is evidence that a large amount of extension is present within this section of the Pacific plate. In our models of plate flexure, if we include the plate interface landward of the trench axis, the best fitting boundary forces acting on the subducting slab favor extensional horizontal and downward vertical forces. Similar results were found by *Garcia-Castellanos et al.* [2000] for the Pacific plate at the

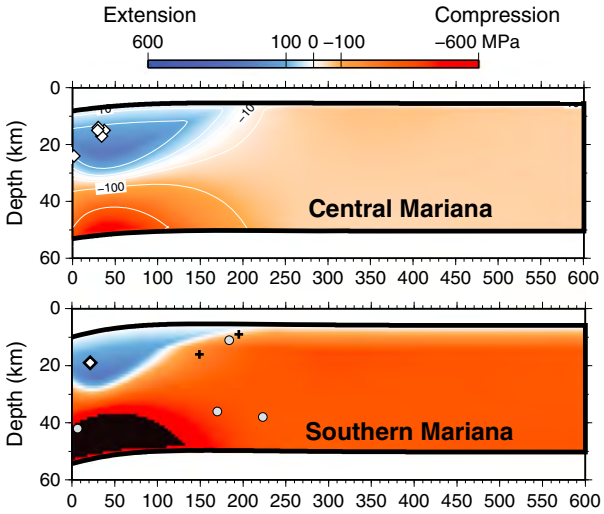

Figure 8. (top) The best fit flexure model for the Central Mariana outer rise using bathymetry seaward (east) of the trench axis. (bottom) The best fit flexure model for the Southern Mariana outer rise using bathymetry seaward (southeast) of the trench axis. Tensional deviatoric stresses correspond to blue regions and positive values (MPa); compression corresponds to red regions and negative values, and black regions indicate highly compressional stresses where the color scale has saturated. Extensional earthquakes plotted as white diamonds; strike-slip earthquakes are black crosses; compressional earthquakes are gray circles.

Tonga-Kermadec subduction zone, and they interpret this tension within the Pacific plate outer rise to be indicative of strong slab pull forces. Given the nearly vertically dipping slab at Central Mariana [*Stern et al*., 2003], strong slab pull forces have been proposed by *Uyeda and Kanamori* [1979] to explain the apparently decoupled plate interface of the Mariana subduction zone.

In this region, none of our modeled plate profiles are able to match the abrupt kink in the plate as observed by *Oakley et al*. [2008]. *Oakley et al*. [2008] interpret this abrupt change in the slope of the plate as an indication that it is faulted completely through. If the plate were faulted through as has been discussed for several other subduction zones [*Kanamori*, 1971; *Abe*, 1972; *Kanamori*, 1972; *Fitch et al*., 1981; *Lynnes and Lay*, 1988; *Kao and Chen*, 1996], then it cannot have a strong elastic core, which is an assumption made by our plate flexure models. The predominance of intermediate and large extensional earthquakes in this region and the indications for failure of the incoming plate appears consistent with the interpretation that the plate interface in Central Mariana is decoupled or weakly coupled [*Uyeda and Kanamori*, 1979]. This interpretation fits with recent studies that find evidence for loss of elasticity within the incoming plate at other subduction zone trenches [*Billen and Gurnis*, 2005; *Arredondo and Billen*, 2012].

In contrast, both extensional and compressional earthquakes are located within the outer rise at southern Mariana. The existence of compressional outer rise earthquakes was suggested by *Christensen and Ruff* [1988] to indicate strong coupling along the shallow subduction plate interface. The island of Guam in fact does have historical indications of strong shaking, although it is not necessarily true that the sources of shaking were large plate interface earthquakes [*Maso*, 1910; *Soloviev and Go*, 1974; *Emry et al*., 2011]. The three $Mw > 7.0$ earthquakes that occurred near Guam in 1993, 2001, and 2002 were initially thought to have occurred along the subduction plate interface (Global CMT catalog) [*Dziewonski et al*., 1981; *Scholz and Campos*, 1995; *Campos et al*., 1996]; however, others have proposed a source within the subducting slab [*Tanioka et al*., 1995; *Harada and Ishibashi*, 2008]. *Scholz and Campos* [1995] proposed that the Southern Mariana plate interface is more strongly coupled than the Central plate interface. Another interpretation to explain the large compressional forces at the trench predicted by flexure models is combined ridge push and mantle drag forces, in contrast to the results from *Garcia-Castellanos et al*. [2000] for the Tonga subduction zone. Questions remain as to whether compressional outer rise earthquakes always indicate strong plate interface coupling; however, based on the agreement between the deep compressional earthquake in our data set and our best fitting flexure models that predict a strongly bending Pacific plate undergoing regional compression, we propose that the Southern Mariana plate interface is more strongly coupled than the Central plate interface and therefore has greater seismic potential in agreement with *Scholz and Campos* [1995].

5.3. Water Inputs at the Mariana Subduction Zone

The depth of extensional and compressional earthquakes combined with models of plate flexure suggests that the maximum depth of extension varies along the length of the Mariana subduction zone. If we assume that faults at depth are connected to fault scarps at the surface (Figures 6, S21–S26, and Text S3) and that extensional earthquakes mark the lower depth to which water can percolate into the bending

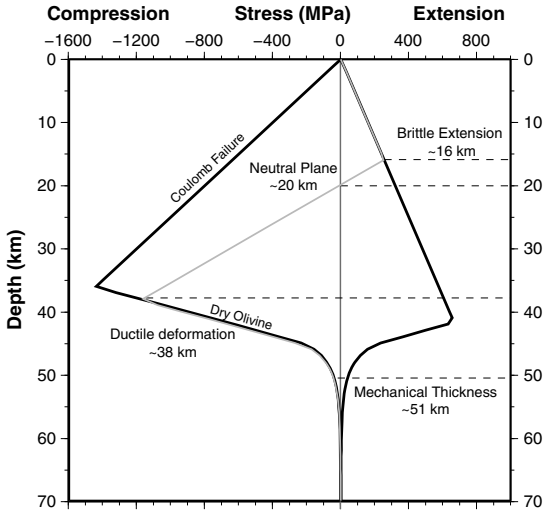

Figure 9. Yield Stress Envelope (YSE) corresponding to the distance of maximum bending moment for the best fitting flexure model in Southern Mariana. *X* axis gives stress values (MPa), compression (negative) to left of the origin and tension (positive) to right of the origin. *Y* axis is depth (km) beneath the top of the plate. Black lines outline failure envelope. Coulomb failure criteria (compression, left; tension, right) extends from the origin to depths of ~40–45 km. Ductile deformation controls deformation to depth of the mechanical thickness ~50 km. Thin gray line shows the 0 MPa trend line and the thick gray line shows the change in stress within the bending plate with depth. Dashed gray lines show depths at which the plate stress switches from brittle failure to elastic core, the neutral plane, the depth where plate stress switches from elastic to ductile deformation, and the mechanical thickness depth.

plate as was assumed by *Ranero et al.* [2003] and *Lefeldt et al.* [2009], then we expect that regions of the Pacific plate with deeper outer rise extension are more pervasively serpentinized (Figure 11).

Van Keken et al. [2011] suggest that the Mariana subduction zone does not subduct a significant amount of water beyond the mantle wedge (deeper than ~250 km), meaning that the majority of water stored within the downgoing plate should be released within the shallow portion of the mantle wedge and beneath the arc. Greater amounts of hydration within the downgoing plate mantle will have a greater effect on the amount of water carried deeper into the subduction zone to depths beyond the volcanic arc [*Hacker*, 2008; *Van Keken et al.*, 2011]. At the Mariana island arc, subaerial arc volcanoes are located only in North Central Mariana (~16–20°N), inboard of the region of greatest extension within the incoming Pacific plate; among these arc volcanoes, there is no clear along-strike trend in amount of water output [*Kelley et al.*, 2006; *Shaw et al.*, 2008; *Kelley et al.*, 2010; *Parman et al.*, 2011]. Back-arc basin basalts from Southern Mariana have higher concentrations of water

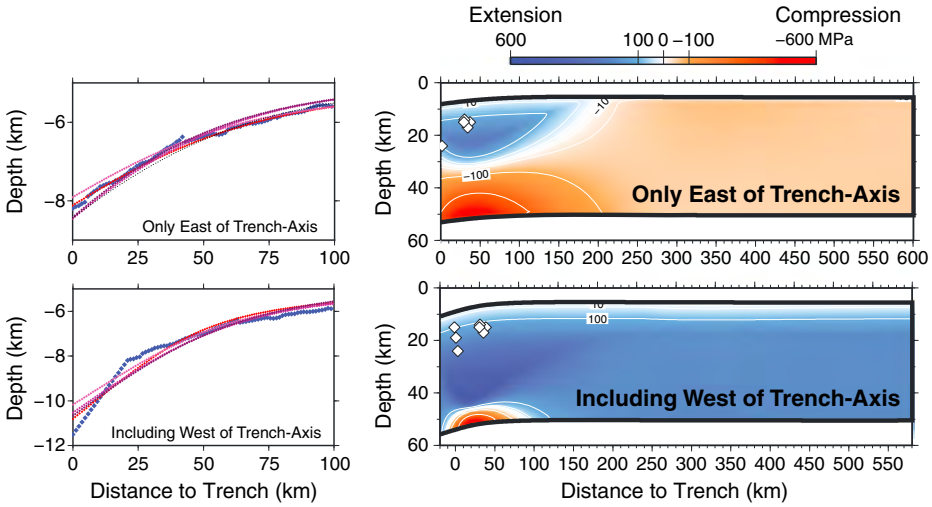

Figure 10. (top right) Stress distribution predicted by best fit flexure model for the North Central Mariana outer rise using bathymetry profile eastward of the trench axis. (bottom right) Best fit model using bathymetry eastward of trench axis and profile of the plate interface westward of the trench axis [*Oakley et al.*, 2008]. The bottom stress distribution is shifted ~20 km westward of top plot, due to inclusion of the plate profile landward of the trench. Extensional stresses correspond to blue regions and positive values (MPa); compression corresponds to red regions and negative values. Extensional earthquakes are plotted as white diamonds; strike-slip earthquakes are black crosses; compressional earthquakes are gray circles. (left column) Observed profile of the top of the plate (from bathymetry or from bathymetry and seismic reflection) is denoted by the thick blue points. The plate profiles predicted by other small misfit flexure models are plotted as shades of red and purple.

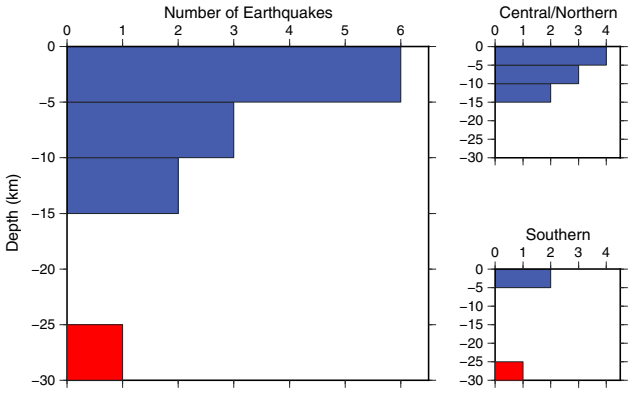

Figure 11. Distribution of earthquakes at Central/Northern Mariana with depth. (left) Depth and number of all events within the incoming Pacific plate mantle at the Mariana subduction zone. Blue bars are extensional earthquakes and red bars are compressional earthquakes. Depth is given as kilometers below the Moho. (top right) Central Mariana earthquakes. (bottom right) Southern Mariana.

in comparison to the Central Mariana trough and are separated from the volcanic arc by much shorter distances [*Fryer et al*., 1998; *Martinez et al*., 2000; *Taylor and Martinez*, 2003, and references therein]; however, no direct comparison of along arc changes in total subduction zone water output has been attempted. Furthermore, obtaining reliable estimates of water concentrations from subduction zone volcanoes that are representative of upper mantle materials continues to be problematic [*Plank et al*., 2013; *Bucholz et al*., 2013].

Flux of water from the downgoing plate is dependent upon many factors, such as initial extent of slab mantle hydration [e.g., *Rüpke et al*., 2004; *Van Keken et al*., 2011], rate of slab subduction and changes in slab mineral assemblages with increasing depth [*Ulmer and Trommsdorf*, 1995; *Rüpke et al*., 2004; *Hacker*, 2008], and degree of localized hydration along faults [*Wada et al*., 2012]. The amount of water carried deeper into the mantle depends critically on the depth and amount of hydration of the subducting oceanic mantle, since most of the water trapped in the sediments and shallow crust is released at shallow depth. Most models calculating global subduction zone water flux assume a homogeneous layer of serpentinized mantle within the subducting slab [*Schmidt and Poli*, 1998; *Jarrard*, 2003; *Rüpke et al*., 2004; *Hacker*, 2008; *Van Keken et al*., 2011], although the actual patterns of hydration are likely heterogeneous and dependent upon the tectonic setting and state of the incoming plate [*Ranero et al*., 2005; *Van Avendonk et al*., 2011]. Our results indicate along-strike changes in maximum depth of extensional earthquakes from greater than 11 km within the mantle at Central Mariana to 5 km in Southern Mariana. Despite the changes along strike, the maximum depth of extensional earthquakes within the incoming plate at Southern and Central Mariana is deeper than the ~2–4 km depth of hydration assumed in recent models [*Hacker*, 2008; *Van Keken et al*., 2011], suggesting that greater hydration is possible along the entire arc.

If we assume that depth of extension in the outer rise reflects depth of mantle serpentinization, our results suggest that at least the upper 11 km of the slab mantle at Central Mariana is hydrated and the top 5 km of slab mantle is hydrated at Southern Mariana. For the 500 km of the Mariana subduction zone corresponding to the region from ~15 to 20°N, *Van Keken et al*. [2011] estimate 21.2 Tg/Myr/m or 10.6E6 Tg/Myr for partial serpentinization to 2 km (2 wt % H_2O) and 44.2 Tg/Myr/m (22E6 Tg/Myr) for full serpentinization. Along the Nicaragua margin, *Van Avendonk et al*. [2011] find evidence for up to ~20–30% serpentinized corresponding to 3–4 wt % H_2O at ~5–10 km within the incoming plate mantle. If we assume the partially serpentinized (2 wt % H_2O) scenario from *Van Keken et al*. [2011] to the depth of our deepest extensional earthquake (11 km in the incoming plate mantle), then the amount of water input into the Mariana subduction zone through mantle serpentinization would be 51 Tg/Myr/m, which is ~2.5 times greater than the partially serpentinized scenario from *Van Keken et al*. [2011]. If the incoming plate mantle holds as much water (~3.5 wt % H_2O) as found at Nicaragua [*Van Avendonk et al*., 2011], then the total amount of serpentinized mantle water contribution is 78 Tg/Myr/m, or almost 4 times larger than the partially serpentinized scenario from *Van Keken et al*. [2011] and 1.75 times larger than their fully serpentinized scenario.

In order to establish a range of slab mantle hydration, given the results from outer rise seismicity, we show several scenarios for water input into the Mariana subduction zone via incoming plate mantle serpentinites (Table 5). Most of the scenarios outlined in Table 5 give a total of ~15–30 $\times$ 10^6 Tg/Myr of water inputted into the South Central Mariana subduction zone, more like the fully serpentinized scenario from *Van Keken et al*. [2011]. There is inherently some uncertainty with estimating the amount of incoming plate mantle hydration based on earthquake depths; however, our results from seismicity provide better constraints on this than were previously available and further illustrates the significant effect that the depth and lateral distribution of mantle serpentinites has on estimates of subduction zone water inputs.

6. Conclusion

Our relative relocations and refined depths of outer rise and outer trench wall earthquakes of moderate to large magnitude occurring during 1990–2011 at the Mariana subduction trench indicate that the Pacific plate undergoes more extensional faulting in the central section of the subduction zone. The observed maximum centroid depth of extensional earthquakes in Central Mariana is 11 km below the Moho. In this region, it is suspected that extensional brittle faulting may extend through the entire thickness of the plate, resulting in a loss of elastic strength, weaker plate interface coupling between the downgoing and overriding plate, existence of large outer rise extensional earthquakes, and likely deeper outer rise mantle serpentinization. In Southern Mariana, fewer moderate to large magnitude extensional earthquakes occur, and the maximum depth for extensional earthquakes near the Southern Mariana trench is ~5 km into the mantle. In addition, a compressional earthquake in this region is located 34 km below the seafloor, suggesting that the neutral plane is elevated and brittle faulting extends into the compressional field. The best fitting models corresponding to the bathymetric profile at Southern Mariana suggest that the plate is undergoing significant regional compression; this coincides well with our extensional and compressional earthquake locations and depths. We interpret these observations to be indicative of a more strongly coupled plate interface in Southern Mariana. Although the relationship between the plate interface seismic cycle and amount of water infiltrating into the bending plate is not well understood, based on the contrast between the two regions, we suggest that the Pacific plate is hydrated to greater depth in the central section of the margin than in Southern Mariana. Furthermore, we propose that the overall amount of hydration within the Mariana subduction zone is likely greater than that assumed by recent models of subduction zone water fluxes due to a larger thickness of the hydrated layer in the mantle.

Acknowledgments

Many thanks to M. Brounce, H. Chou, J. Conder, K. Kelley, D. Lizarralde, F. Martinez, B. Savage, B. Shiro, P. Shore, P. Skemer, S. Solomatov, S. Stein, R. Stern, and L. Warren for beneficial discussions and technical assistance. Helpful feedback provided by B. Savage, W.P. Schellart, and an anonymous reviewer improved the quality of this paper and is much appreciated. Thank you to the IRIS Data Management Center, which provided access to the waveform data used in this study. Support for this research was provided under NSF grants OCE-0426408, OCE-0752476, and OCE-0841074. Additional funding to present this research was provided by the NSF Earthscope and GeoPRISMs programs as well as the NSF/FESD CIDER program (NSF/EAR-1135452). Maps and cross sections were created using the GMT software [*Wessel and Smith*, 1991].

References

Abe, K. (1972), Lithospheric normal faulting beneath the Aleutian trench, *Phys. Earth Planet. Inter.*, *5*, 190–198, doi:10.1016/0031-9201(72)90091-X.

Ammon, C. J., H. Kanamori, and T. Lay (2008), A great earthquake doublet and seismic stress transfer cycle in the central Kuril islands, *Nature*, *451*(7178), 561–566, doi:10.1038/nature06521.

Arredondo, K. M., and M. I. Billen (2012), Rapid weakening of subducting plates from trench-parallel estimates of flexural rigidity, *Phys. Earth Planet. Int.*, *196–197*, 1–13, doi:10.1016/j.pepi.2012.02.007.

Audet, P., M. G. Bostock, N. I. Christensen, and S. M. Peacock (2009), Seismic evidence for overpressured subducted oceanic crust and megathrust fault sealing, *Nature*, *457*(7225), 76–78, doi:10.1038/nature07650.

Barklage, M. (2010), Structure and seismicity of the upper mantle using deployments of broadband seismographs in Antarctica and the Mariana Islands, PhD dissertation, 115 pp, Washington University in Saint Louis, Saint Louis.

Billen, M. I., and M. Gurnis (2005), Constraints on subducting plate strength within the Kermadec trench, *J. Geophys. Res.*, *110*, B05407, doi:10.1029/2004JB003308.

Bucholz, C. E., G. A. Gaetani, M. D. Behn, and N. Shimizu (2013), Post-entrapment modification of volatiles and oxygen fugacity in olivine-hosted melt inclusions, *Earth Planet. Sci. Lett.*, *374*, 145–155, doi:10.1016/j.epsl.2013.05.033.

Caldwell, J. G., W. F. Haxby, D. E. Karig, and D. L. Turcotte (1976), On the applicability of a universal elastic trench profile, *Earth Planet. Sci. Lett.*, *31*, 239–246, doi:10.1016/0012-821X(76)90215-6.

Campos, J., R. Madariaga, and C. Scholz (1996), Faulting processes of the August 8, 1993, Guam earthquake: A thrust event in an otherwise weakly coupled subduction zone, *J. Geophys. Res.*, *101*(B8), 17,581–17,596, doi:10.1029/96JB00654.

Chapple, W. M., and D. W. Forsyth (1979), Earthquakes and bending of plates at trenches, *J. Geophys. Res.*, *84*(B12), 6729–6749, doi:10.1029/JB084iB12p06729.

Christensen, D. H., and L. J. Ruff (1988), Seismic coupling and outer rise earthquakes, *J. Geophys. Res.*, *93*(B11), 13,421–13,444, doi:10.1029/JB093iB11p13421.

Contreras-Reyes, E., I. Grevemeyer, E. R. Flueh, M. Scherwath, and M. Heesemann (2007), Alteration of the subducting oceanic lithosphere at the southern central Chile trench-outer rise, *Geochem. Geophys. Geosyst.*, *8*, Q07003, doi:10.1029/2007GC001632.

Dziewonski, A. M., T. A. Chou, and J. H. Woodhouse (1981), Determination of earthquake source parameters from waveform data for studies of global and regional seismicity, *J. Geophys. Res.*, *86*(B4), 2825–2852, doi:10.1029/JB086iB04p02825.

Ekström, G., M. Nettles, and A. M. Dziewoński (2012), The global CMT project 2004–2010: Centroid-moment tensors for 13,017 earthquakes, *Phys. Earth Planet. Int.*, *200–201*, 1–9, doi:10.1016/j.pepi.2012.04.002.

Emry, E. L., D. A. Wiens, H. Shiobara, and H. Sugioka (2011), Seismogenic characteristics of the Northern Mariana shallow thrust zone from local array data, *Geochem. Geophys. Geosyst.*, *12*, Q12008, doi:10.1029/2011GC003853.

Faccenda, M., T. V. Gerya, and L. Burlini (2009), Deep slab hydration induced by bending-related variations in tectonic pressure, *Nat. Geosci.*, *2*, 790–793, doi:10.1038/NGEO656.

Fitch, T. J., R. G. North, and M. W. Shields (1981), Focal depths and moment tensor representations of shallow earthquakes associated with the Great Sumba Earthquake, *J. Geophys. Res.*, *86*(B10), 9357–9374, doi:10.1029/JB086iB10p09357.

Fryer, P., H. Fujimoto, M. Sekine, L. E. Johnson, J. Kasahara, H. Masuda, T. Gamo, T. Ishii, M. Ariyoshi, and K. Fujioka (1998), Volcanoes of the southwestern extension of the active Mariana island arc: New swath-mapping and geochemical studies, *Island Arc*, *7*, 596–607, doi:10.1111/j.1440-1738.1998.00212.x.

Fryer, P., C. G. Wheat, and M. J. Mottl (1999), Mariana blueschist mud volcanism: Implications for conditions within the subduction zone, *Geology*, *27*(2), 103–106, doi:10.1130/0091-7613(1999)027<0103:MBMVIF>2.3.CO;2.

Garcia-Castellanos, D., M. Fernàndez, and M. Torne (1997), Numerical modeling of foreland basin formation: A program relating thrusting, flexure, sediment geometry and lithosphere rheology, *Comput. Geosci.*, *23*(9), 993–1003, doi:10.1016/S0098-3004(97)00057-5.
Garcia-Castellanos, D., M. Torne, and M. Fernàndez (2000), Slab pull effects from a flexural analysis of the Tonga and Kermadec trenches (Pacific Plate), *Geophys. J. Int.*, *141*(2), 479–484, doi:10.1046/j.1365-246x.2000.00096.x.
Gardner, J. V. (2010), U.S. Law of the Sea cruises to map sections of the Mariana Trench and the eastern and southern insular margins of Guam and the Northern Mariana Islands, *Rep. UNH-CCOM/JHC Technical Report 10-003*.
Gill, J. B. (1981), *Orogenic Andesites and Plate Tectonics*, pp. 390, Springer, New York.
Goetze, C. (1978), The mechanisms of creep in olivine, *Phil. Trans. R. Soc. London*, *288*, 99–119, doi:10.1098/rsta.1978.0008.
Goetze, C., and B. Evans (1979), Stress and temperature in the bending lithosphere as constrained by experimental rock mechanics, *Geophys. J. R. Astron. Soc.*, *59*(3), doi:10.1111/j.1365-246X.1979.tb02567.x.
Hacker, B. R. (2008), H_2O subduction beyond arcs, *Geochem. Geophys. Geosyst.*, *9*, Q03001, doi:10.1029/2007GC001707.
Harada, T., and K. Ishibashi (2008), Interpretation of the 1993, 2001, and 2002 Guam earthquakes as intraslab events by a simultaneous relocation of the mainshocks, aftershocks, and background earthquakes, *Bull. Seismol. Soc. Am.*, *98*(3), 1581–1587, doi:10.1785/0120060227.
Hirschmann, M. M. (2006), Water, melting, and the deep Earth H_2O cycle, *Annu. Rev. Earth Planet. Sci.*, *34*, 629–653, doi:10.1146/annurev.earth.34.031405.125211.
International Seismological Centre *On-line Bulletin* (2010), http://www.isc.ac.uk, Internatl. Seis. Cent., Thatcham, U. K.
Isacks, B., J. Oliver, and L. R. Sykes (1968), Seismology and the new global tectonics, *J. Geophys. Res.*, *73*(18), 5855–5899, doi:10.1029/JB073i018p05855.
Ivandic, M., I. Grevemeyer, J. Bialas, and C. J. Petersen (2010), Serpentinization in the trench-outer rise region offshore of Nicaragua: Constraints from seismic refraction and wide-angle data, *Geophys. J. Int.*, *180*, 1253–1264, doi:10.1111/j.1365-246X.2009.04474.x.
Jarrard, R. D. (2003), Subduction fluxes of water, carbon dioxide, chlorine, and potassium, *Geochem. Geophys. Geosyst.*, *4*(5), 8905, doi: 10.1029/2002GC000392.
Jordan, T. H., and K. A. Sverdrup (1981), Teleseismic location techniques and their application to earthquake clusters in the South-Central Pacific, *Bull. Seismol. Soc. Am.*, *71*(4), 1105–1130.
Kanamori, H. (1971), Seismological evidence for a lithospheric normal faulting—The Sanriku earthquake of 1933, *Phys. Earth Planet. Inter.*, *4*(4), 289–300, doi:10.1016/0031-9201(71)90013-6.
Kanamori, H. (1972), Mechanism of tsunami earthquakes, *Phys. Earth Planet. Inter.*, *6*, 346–359, doi:10.1016/0031-9201(72)90058-1.
Kanamori, H., and D. Anderson (1975), Theoretical basis of some empirical relations in seismology, *Bull. Seismol. Soc. Am.*, *65*(5), 1073–1095.
Kao, H., and W.-P. Chen (1996), Seismicity in the outer rise–forearc region and configuration of the subducting lithosphere with special reference to the Japan Trench, *J. Geophys. Res.*, *101*(B12), 27,811–27,831, doi:10.1029/96JB01760.
Kato, T., J. Beavan, T. Matsushima, Y. Kotake, J. T. Camacho, and S. Nakao (2003), Geodetic evidence of back-arc spreading in the Mariana Trough, *Geophys. Res. Lett.*, *30*(12), 1625, doi: 10.1029/2002GL016757.
Katsumata, M., and L. R. Sykes (1969), Seismicity and tectonics of the western Pacific: Izu-Mariana-Caroline and Ryuku-Taiwan regions, *J. Geophys. Res.*, *74*(25), 5923–5948, doi:10.1029/JB074i025p05923.
Kelley, K. A., T. Plank, T. L. Grove, E. M. Stolper, S. Newman, and E. Hauri (2006), Mantle melting as a function of water content beneath back-arc basins, *J. Geophys. Res.*, *111*, B09208, doi:10.1029/2005JB003732.
Kelley, K. A., T. Plank, S. Newman, E. M. Stolper, T. L. Grove, S. Parman, and E. H. Hauri (2010), Mantle melting as a function of water content beneath the Mariana Arc, *J. Petrol.*, *51*(8), 1711–1738, doi:10.1093/petrology/egq036.
Kennett, B. L. N., and E. R. Engdahl (1991), Traveltimes for global earthquake location and phase identification, *Geophys J. Int.*, *105*(2), 429–465, doi:10.1111/j.1365-246X.1991.tb06724.x.
Kikuchi, M., and H. Kanamori (1991), Inversion of complex body waves—III, *Bull. Seismol. Soc. Am.*, *81*(6), 2335–2350.
Korenaga, J. (2007), Thermal cracking and the deep hydration of oceanic lithosphere: A key to the generation of plate tectonics?, *J. Geophys. Res.*, *112*, B05408, doi:10.1029/2006JB004502.
Langston, C. A., and D. V. Helmberger (1975), A procedure for modeling shallow dislocation sources, *Geophys. J. R. Astron. Soc.*, *42*(1), 117–130, doi:10.1111/j.1365-246X.1975.tb05854.x.
Lay, T., H. Kanamori, C. J. Ammon, A. R. Hutko, K. Furlong, and L. Rivera (2009), The 2006–2007 Kuril Islands great earthquake sequence, *J. Geophys. Res.*, *114*, B11308, doi:10.1029/2008JB006280.
Lay, T., C. J. Ammon, H. Kanamori, L. Rivera, K. D. Koper, and A. R. Hutko (2010), The 2009 Samoa-Tonga great earthquake triggered doublet, *Nature*, *466*, 964–968, doi:10.1038/nature09214.
Lefeldt, M., I. Grevemeyer, J. Goßler, and J. Bialas (2009), Intraplate seismicity and related mantle hydration at the Nicaraguan trench outer rise, *Geophys. J. Int.*, *178*(2), 742–752, doi:10.1111/j.1365-246X.2009.04167.x.
Lynnes, C. S., and T. Lay (1988), Source process of the great 1977 Sumba earthquake, *J. Geophys. Res.*, *93*(B11), 13,407–13,420, doi:10.1029/JB093iB11p13407.
Martinez, F., P. Fryer, and N. Becker (2000), Geophysical characteristics of the southern Mariana Trough, 11°50′N–13°40′N, *J. Geophys. Res.*, *105*(B7), 16,591–16,607, doi:10.1029/2000JB900117.
Martinez, F., K. A. Kelley, and R. J. Stern (2012), Creation and deformation of hydrous lithosphere at the Southern Mariana margin, *Geophys. Res. Abstr.*, *14*, EGU2012–6643.
Maso, M. S. (1910), *Catalogue of Violent and Destructive Earthquakes in the Philippines. With an appendix: Earthquakes in the Marianas Islands, 1599–1909*, Philippine Island Weather Bureau, Manila.
Masson, D. G. (1991), Fault patterns at outer trench walls, *Mar. Geophys. Res.*, *13*(3), 209–225, doi:10.1007/BF00369150.
McNutt, M. K. (1984), Lithospheric flexure and thermal anomalies, *J. Geophys. Res.*, *89*(B13), 11,180–11,194, doi:10.1029/JB089iB13p11180.
Meade, C., and R. Jeanloz (1991), Deep-focus earthquakes and recycling of water into the Earth's mantle, *Science*, *252*(5002), 68–72, doi:10.1126/science.252.5002.68.
Moore, J. C., and P. Vrolijk (1992), Fluids in accretionary prisms, *Rev. Geophys.*, *30*(2), 113–135, doi:10.1029/92RG00201.
National Geophysical Data Center (2006), 2-minute Gridded Global Relief Data (ETOPO2v2). U.S. Department of Commerce, National Oceanic and Atmospheric Administration. [Available at http://www.ngdc.noaa.gov/mgg/fliers/06mgg01.html.]
Oakley, A. J., B. Taylor, and G. F. Moore (2008), Pacific Plate subduction beneath the central Mariana and Izu-Bonin fore arcs: New insights from an old margin, *Geochem. Geophys. Geosyst.*, *9*, Q06003, doi:10.1029/2007GC001820.
Okal, E. A., D. Reymond, and S. Hongsresawat (2013), Large, pre-digital earthquakes of the Bonin-Mariana subduction zone, *Tectonophysics*, *586*, 1–14, doi:10.1016/j.tecto.2012.09.006.
O'Neill, C., A. M. Jellinek, and A. Lenardic (2007), Conditions for the onset of plate tectonics on terrestrial planets and moons, *Earth Planet. Sci. Lett.*, *261*, 20–32, doi:10.1016/j.epsl.2007.05.038.

Parman, S. W., T. L. Grove, K. A. Kelley, and T. Plank (2011), Along-arc variations in the pre-eruptive H_2O contents of Mariana arc magmas inferred from fractionation paths, *J. Petrol.*, *52*(2), 257–278, doi:10.1093/petrology/egq079.

Parsons, B., and J. G. Sclater (1977), An analysis of the variation of ocean floor bathymetry and heat flow with age, *J. Geophys. Res.*, *82*(5), 803–827, doi:10.1029/JB082i005p00803.

Phipps Morgan, J., and B. K. Holtzman (2005), Vug waves: A mechanism for coupled rock deformation and fluid migration, *Geochem. Geophys. Geosyst.*, *6*Q08002, doi:10.1029/2004GC000818.

Plank, T., and C. H. Langmuir (1993), Tracing trace elements from sediment input to volcanic output at subduction zones, *Nature*, *362*, 739–743, doi:10.1038/362739a0.

Plank, T., K. A. Kelley, M. M. Zimmer, E. H. Hauri, and P. J. Wallace (2013), Why do mafic magmas contain ~4 wt % water on average?, *Earth Planet. Sci. Lett.*, *364*, 168–179, doi:10.1016/j.epsl.2012.11.044.

Pozgay, S., D. A. Wiens, J. A. Conder, H. Shiobara, and H. Sugioka (2009), Seismic attenuation tomography of the Mariana arc: Implications for thermal structure, volatile distribution, and dynamics, *Geochem. Geophys. Geosyst.*, *10*, Q04X05, doi:10.1029/2008GC002313.

Pyle, M., D. A. Wiens, D. S. Weeraratne, P. J. Shore, H. Shiobara, and H. Sugioka (2010), Shear velocity structure of the Mariana mantle wedge from Rayleigh wave phase velocities, *J. Geophys. Res.*, *115*, B11304, doi:10.1029/2009JB006976.

Raeesi, M., and K. Atakan (2009), On the deformation cycle of a strongly coupled plate interface: The triple earthquakes of 16 March 1963, 15 November 2006, and 13 January 2007 along the Kurile subduction zone, *J. Geophys. Res.*, *114*, B10301, doi:10.1029/2008JB006184.

Raleigh, C. B., and M. S. Paterson (1965), Experimental deformation of serpentinite and its tectonic implications, *J. Geophys. Res.*, *70*(16), 3965–3985, doi:10.1029/JZ070i016p03965.

Ranero, C. R., J. Phipps Morgan, K. McIntosh, and C. Reichert (2003), Bending-related faulting and mantle serpentinization at the Middle America trench, *Nature*, *425*(6956), 367–373, doi:10.1038/nature01961.

Ranero, C. R., A. Villasenor, J. P. Morgan, and W. Weinrebe (2005), Relationship between bend-faulting at trenches and intermediate-depth seismicity, *Geochem. Geophys. Geosyst.*, *6*, Q12002, doi:10.1029/2005GC000997.

Rüpke, L. H., J. Phipps Morgan, M. Hort, and J. A. D. Connolly (2004), Serpentine and the subduction zone water cycle, *Earth Planet. Sci. Lett.*, *223*(1–2), 17–34, doi:10.1016/j.epsl.2004.04.018.

Satake, K., Y. Yoshida, and K. Abe (1992), Tsunami from the Mariana earthquake of April 5, 1990—Its abnormal propagation and implications for tsunami potential from outer-rise earthquakes, *Geophys. Res. Lett.*, *19*(3), 301–304, doi:10.1029/91GL02493.

Savage, B. (2012), Seismic constraints on the water flux delivered to the deep Earth by subduction, *Geology*, *40*(3), 235–238, doi:10.1130/G32499.1.

Schmidt, M. W., and S. Poli (1998), Experimentally based water budgets for dehydrating slabs and consequences for arc magma generation, *Earth Planet. Sci. Lett.*, *163*(1-4), 361–379, doi:10.1016/S0012-821X(98)00142-3.

Scholz, C. H., and J. Campos (1995), On the mechanism of seismic decoupling and back arc spreading at subduction zones, *J. Geophys. Res.*, *100*(B11), 22,103–22,115.

Shaw, A. M., E. H. Hauri, T. P. Fischer, D. R. Hilton, and K. A. Kelley (2008), Hydrogen isotopes in Mariana arc melt inclusions: Implications for subduction dehydration and the deep-Earth water cycle, *Earth Planet. Sci. Lett.*, *275*(1–2), 138–145, doi:10.1016/j.epsl.2008.08.015.

Shelly, D. R., G. C. Beroza, S. Ide, and S. Nakamula (2006), Low-frequency earthquakes in Shikoku, Japan, and their relationship to episodic tremor and slip, *Nature*, *442*(7099), 188–191, doi:10.1038/nature04931.

Sibson, R. H. (1994), Crustal stress, faulting and fluid flow, in *Geofluids: Origin, Migration and Evolution of Fluids in Sedimentary Basins*, *Geol. Soc. Spec. Publ.*, vol. 78, edited by J. Parnell, pp. 69-84, Geological Society, London, doi: 10.1144/GSL.SP.1994.0.78.01.07.

Soloviev, S. L. and C. N. Go (1974), *A Catalogue of Tsunamis on the Western Shore of the Pacific Ocean [in Russian], Nauka, Moscow*. [English translation, Can. Transl., Fish Aquat. Sci., vol. 5077, 447 pp., Inst. Ocean Sci., Sidney, B.C., Canada, 1984].

Stauder, W. (1968), Mechanism of the Rat Island earthquake sequence of February 4, 1965, with relation to island arcs and sea-floor spreading, *J. Geophys. Res.*, *73*(12), 3847–3858, doi:10.1029/JB073i012p03847.

Stein, C. A., and S. Stein (1992), A model for the global variation in oceanic depth and heat flow with lithospheric age, *Nature*, *359*(6391), 123–129, doi:10.1038/359123a0.

Stern, R. J., M. J. Fouch, and S. L. Klemperer (2003), An overview of the Izu-Bonin-Mariana subduction factory, in *Inside the Subduction Factory*, *Geophys. Monogr. Ser.*, vol. 138, edited by J. M. Eiler, pp. 175-222, AGU, Washington, D. C, doi:10.1029/138GM10.

Takahashi, N., S. Kodaira, S. L. Klemperer, Y. Tatsumi, Y. Kaneda, and K. Suyehiro (2007), Crustal structure and evolution of the Mariana intra-oceanic island arc, *Geology*, *35*(3), 203–206, doi:10.1130/G23212A.1.

Tanioka, Y., K. Satake, and L. Ruff (1995), Analysis of seismological and tsunami data from the 1993 Guam Earthquake, *Pure Appl. Geophys.*, *144*(3–4), 823–837, doi:10.1007/BF00874396.

Taylor, B., and F. Martinez (2003), Back-arc basin basalt systematics, *Earth Planet. Sci. Lett.*, *210*, 481–497, doi:10.1016/S0012-821X(03)00167-5.

Thompson, A. B. (1992), Water in the Earth's upper mantle, *Nature*, *358*(6384), 295–302, doi:10.1038/358295a0.

Tibi, R., D. A. Wiens, and X. Yuan (2008), Seismic evidence for widespread serpentinized forearc mantle along the Mariana convergence margin, *Geophys. Res. Lett.*, *35*, L13303, doi:10.1029/2008GL034163.

Ulmer, P., and V. Trommsdorf (1995), Serpentine stability to mantle depths and subduction-related magmatism, *Science*, *268*(5212), 858–861, doi:10.1126/science.268.5212.858.

Uyeda, S., and H. Kanamori (1979), Back-arc opening and the mode of subduction, *J. Geophys. Res.*, *84*(B3), 1049–1061, doi:10.1029/JB084iB03p01049.

Van Avendonk, H. J. A., W. S. Holbrook, D. Lizarralde, and P. Denyer (2011), Structure and serpentinization of the subducting Cocos plate offshore Nicaragua and Costa Rica, *Geochem. Geophys. Geosyst.*, *12*, Q06009, doi:10.1029/2011GC003592.

Van Keken, P. E., B. R. Hacker, E. M. Syracuse, and G. A. Abers (2011), Subduction factory: 4. Depth-dependent flux of H_2O from subducting slabs worldwide, *J. Geophys. Res.*, *116*, B01401, doi:10.1029/2010JB007922.

Wada, I., M. D. Behn, and A. M. Shaw (2012), Effects of heterogeneous hydration in the incoming plate, slab rehydration, and mantle wedge hydration on slab-derived H2O flux in subduction zones, *Earth Planet. Sci. Lett.*, *353*, 60–71, doi:10.1016/j.epsl.2012.07.025.

Waschbusch, P. J., and L. H. Royden (1992), Spatial and temporal evolution of foredeep basins: Lateral strength variations and inelastic yielding in continental lithospheres, *Basin Res.*, *4*, 179–195, doi:10.1111/j.1365-2117.1992.tb00044.x.

Wessel, P. (2001), Global distribution of seamounts inferred from gridded Geosat/ERS-1 altimetry, *J. Geophys. Res.*, *106*(B9), 19,431–19,441, doi:10.1029/2000JB000083.

Wessel, P., and W. H. F. Smith (1991), Free software helps map and display data, *EOS Trans. AGU*, *72*, 441.

Yoshida, Y., K. Satake, and K. Abe (1992), The large normal-faulting Mariana earthquake of April 5, 1990 in uncoupled subduction zone, *Geophys. Res. Lett.*, *19*(3), 297–300, doi:10.1029/92GL00165.

Zhang, J. J., and T. Lay (1992), The April 5, 1990 Mariana Islands earthquake and subduction zone stresses, *Phys. Earth Planet. Int.*, *72*(1–2), 99–121, doi:10.1016/0031-9201(92)90052-W.